UiT
THE ARCTIC UNIVERSITY OF NORWAY

Faculty of Science and Technology

Department of Geology

Paleoenvironmental investigation of the northern flank of the Olga Basin (Barents Sea) during the Late Weichselian deglaciation

Jay Patel

Master thesis in Geology [GEO-3900]
June 2018

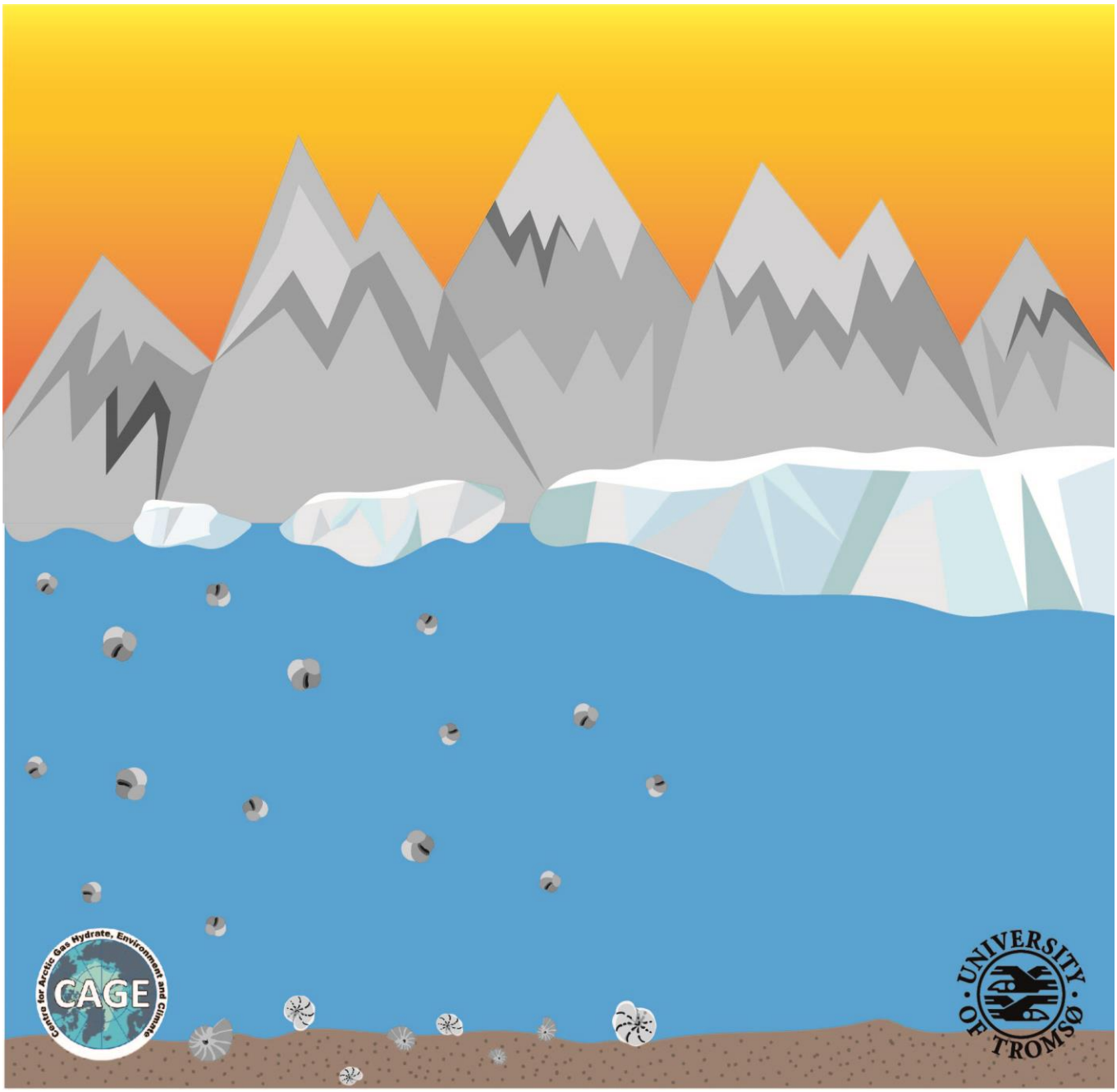

Abstract

Three gravity cores were collected from an unexplored site in the northern flank of the Olga Basin, Barents Sea. The lack of data from the central Barents Sea prompted this investigation and led to defining the evolution of the environment and ice sheet transitions over the Holocene. The three cores underwent benthic foraminiferal studies in combination with stable isotope analysis of ($\delta^{18}O$ and $\delta^{13}C$) *Neogloboquadrina pachyderma*, organic compounds and, element geochemistry of sediments and AMS radiocarbon dating of two samples. Two units were identified, Unit 1 found in the upper section of the cores acquired an AMS dating of 9730 ±40 before present (BP) at its base and is recognised as Holocene sediments. Unit 2 is found in the lower section of the cores and is linked to the Late Weichselian. Most of this unit is barren, containing no foraminifera, and along with the presence of ice rafted debris (IRD) it was interpreted as having permanent ice cover and low oxygen due to pyrite minerals found in the sediment. Low Ca/Ti ratio and rising water content marked a transition phase from permanent ice cover in the Late Weichselian to seasonal ice cover in the Holocene. This resulted in finer terrigenous material with higher organic matter content being deposited in Unit 1. The high biological productivity in Unit 1 can be associated with the Atlantic and Arctic waters.

Acknowledgements

This research was supported by CAGE (Centre for Arctic Gas Hydrate, Environment and Climate) and the Norwegian Petroleum Directorate (NPD).

I would firstly like to express my deep gratitude to my supervisor Giuliana Panieri, for the opportunity to write my master thesis with CAGE and for her expertise and guidance throughout this project. A big thank you goes out to my co-supervisor, Pierre-Antoine Dessandier for his undivided attention and patience throughout this process, even when he was expecting his first child, congratulations!

I am very grateful for the help and guidance from the laboratory staff, Trine Dahl, Ingvild Hald and Karina Monsen who made me feel very welcome and were always there to answer my questions.

Finally, I would like to thank my friends and family for their support and encouragement during my studies and Masha Tsfasman for her soothing presence and helpful advice. Most importantly I wish to thank my parents for bringing me into this world and providing me with every opportunity possible, thank you!

Jay Patel
June 2018

Table of Contents

1. Introduction **1**

1.1. Objective 1

1.2. Study area 1

1.3. Oceanography 2

1.4. Glacial and regional setting 4

1.5. The use of proxies 5

1.5.1. Benthic foraminifera 6

1.5.2. Stable Isotopes of oxygen and carbon in Neogloboquadrina pachyderma 7

1.5.3. Organic Compounds of carbon and nitrogen 8

1.5.4. Chemical compound of sediments 9

2. Materials and methods 10

2.1. Gravity cores 10

2.2. Micropaleontological investigation 11

2.3. Stable isotope analysis 12

2.4. Organic compound analysis 15

2.5. X-ray fluorescence (XRF) analysis 16

2.6. Radiocarbon dating 17

3. Results 19

3.1. Foraminiferal distribution 19

3.1.1. Core HH17-2-935 GC 22

3.1.1.1. Dominant species 22

3.1.2. Core HH17-2-971 GC 22

3.1.2.1. Dominant species 23

3.1.3. Core HH17-2-972 GC 23

3.1.3.1. Dominant species 24

3.2. Stable isotopes: Oxygen and Carbon in *Neogloboquadrina pachyderma* 31

3.2.1. Core HH17-2-935 GC 31

3.2.2. Core HH17-2-971 GC 32

3.2.3. Core HH17-2-972 GC 32

3.3. Organic compounds 34
3.3.1. Core HH17-2-935 GC 34
3.3.2. Core HH17-2-971 GC 35
3.3.3. Core HH17-2-972 GC 35
3.4. X-ray fluorescence (XRF) 37
3.4.1. Core HH17-2-935 GC 35
3.4.2. Core HH17-2-971 GC 35
3.4.3. Core HH17-2-972 GC 35
4. Discussion and interpretation 41
4.1. Foraminifera association 41
4.2. Paleoenvironment reconstruction 48
4.2.1. Unit 2 49
4.2.2. Unit 1 55
4.3. Ice Sheets 58
4.3.1. Late Weichselian Glaciation 58
4.3.2. Holocene 62
5. Summary and conclusion 63
References 65

1. Introduction

1.1. Objective

The objective of this study is to complete a paleoenvironmental investigation of an unexplored site in the northern flank of the Olga Basin, Barents Sea, using 3 gravity cores HH935, HH971 and HH972. Due to lack of data from the central Barents Sea area, these cores can be correlated with other investigations on the continental shelf. The two depressions from where the cores were collected provide the perfect location for gravity coring since sediment accumulation elsewhere is scarce. Several geochemical, sedimentary and faunal parameters were analysed to construct an overview of the study area and contribute in defining the evolution of the environment and ice sheet transitions over the Holocene.

1.2. Study area

Three gravity cores were collected from two topographic depressions (D1 and D2) in the northern flank of the Olga basin in the Barents Sea at approximately 200 m water depth (Fig. 1b). The Barents Sea is the largest inland sea in the world and is

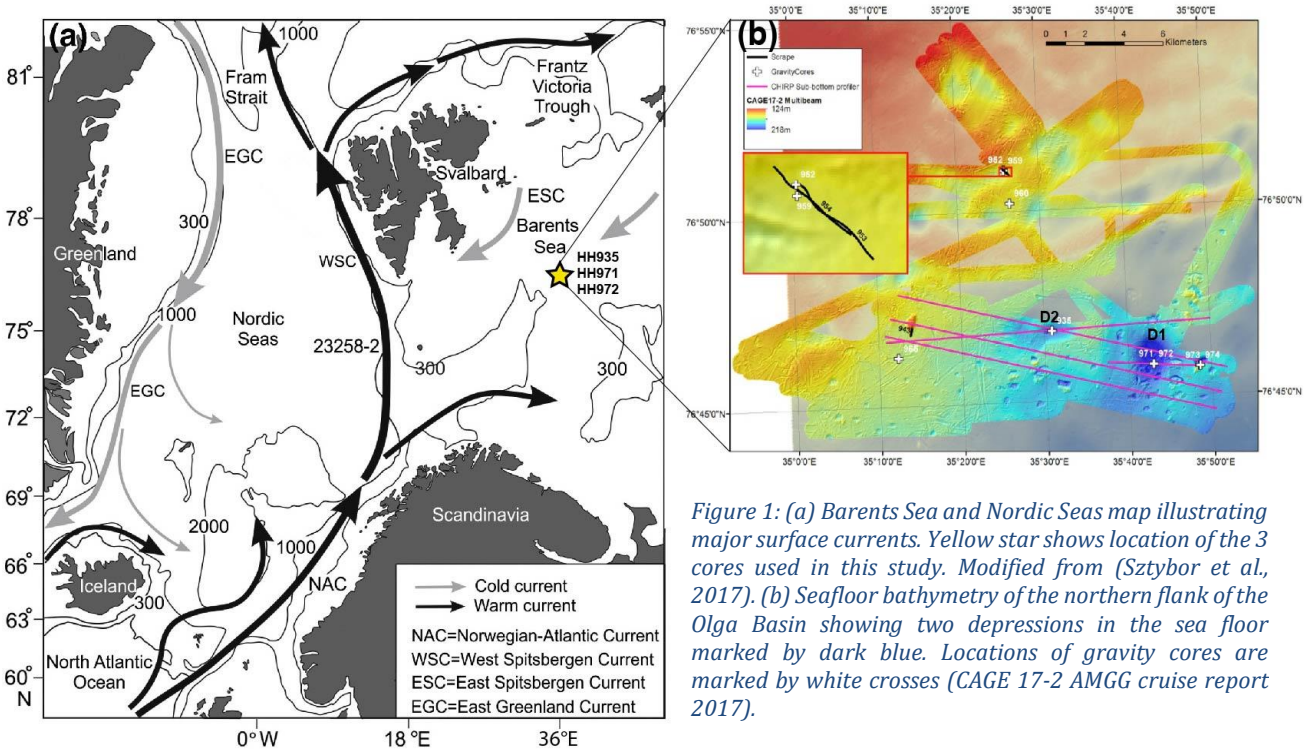

Figure 1: (a) Barents Sea and Nordic Seas map illustrating major surface currents. Yellow star shows location of the 3 cores used in this study. Modified from (Sztybor et al., 2017). (b) Seafloor bathymetry of the northern flank of the Olga Basin showing two depressions in the sea floor marked by dark blue. Locations of gravity cores are marked by white crosses (CAGE 17-2 AMGG cruise report 2017).

defined by its shallow banks, approximately 100-200 m depth and deep troughs, 300-500 m depth (Esteves *et al.*, 2017). These two depressions did not show any sign of gas flares during the CAGE 17-2 survey, but gas flares were identified towards the west and north-west of the depressions (Fig. 2). Bathymetry data in Figure 1b and 2 show plough marks on the sea floor orientated North-South and North east – South west. The East-West trending Olga Basin is located between 76 and 77°N at approximately 35°E in between Storbanken and Sentralbanken. This basin may host the largest post-Jurassic sedimentary rock succession in the NW Barents Sea with relatively undisturbed shallow marine deposits of >750 m. This succession is formed of three types of sandstone: subarkose-sublitharenite, litharenite, and lithic arkose (Antonsen *et al.,* 1991). Holocene mud was measured to be < 0.5 m thick (Antonsen *et al.,* 1991). Sediments within the largest crater (D1) were up to 15 m thick (CAGE 17-2 AMGG cruise report 2017).

1.3. Oceanography

As seen in Figure 1a, currents in the southern part of the Barents Sea flow towards the east and currents in the northern part flow to the west. The three main water masses that characterize the Barents Sea are the coastal water, Atlantic water and Arctic water (Steinsund *et al.,* 1994). The Atlantic water and Coastal water have similar temperatures of 3.5-6.5°C depending on the season but different salinity levels, Coastal water has a salinity <34.7 (Loeng, 1991). Arctic water has low salinity with temperatures <0 °C (Table 1). This study area is found close to the Polar front

Names of the water masses		Characteristics of the water masses	
		T,°C	S
Main water masses:			
Coastal Water	(CW)	>2.0	<34.7
(North) Atlantic Water	(NAW)	>3.0	>35.0
Arctic Water	(AW)	<0.0	34.3–34.8
Locally formed water masses:			
Melt Water	(MW)	>0.0	<34.2
Spitsbergenbanken Water	(SBW)	1.0–3.0	<34.4
Bottom Water	(BW)	<−1.5	>35.0
Barents Sea Water	(BSW)	−1.5–2.0	34.7–35.0
Polar Front Water	(PW)	−0.5–2.0	34.8–35.0

Table 1: Water masses in the Barents Sea and their temperatures and salinity (Loeng, 1991)

where Arctic water meets and mixes with Atlantic water and has the same characteristics as the Barents Sea water but is located in the west (Loeng, 1991). The North Atlantic Current (NAC) transports warm, saline (35‰) water into the Barents Sea along the Norwegian coast has been found as far as Franz Josef Land (78.5°N) (Steinsund *et al.,* 1994) (Fig 1a). The NAC flows into the Arctic Ocean through the Fram Strait and the West Spitsbergen Current (WSC) transports heat and salt resulting in the Fram Strait remaining ice free most of the year (Aagaard *et al.* 1987). As the WSC continues north, it splits into the Yermak Slope Current and the Svalbard Branch (Sztybor and Rasmussen, 2017). Cold currents flow into the Barents Sea from the Arctic Ocean when the sea ice melts in the summer. This flow occurs between Svalbard and Franz Josef Land and is known as the East Spitsbergen Current (ESC) (Fig 1a.), another flow also occurs between Franz Josef Land and Novaya Zemlya. The Barents Sea is situated on a shallow continental shelf with an average depth of 230 m (Loeng, 1991). The deepest area is at 500 m depth, which is located in the western part of the Bjørnøyrenna channel where the NAC flows into the Barents Sea and the shallowest parts are found around Spitsbergenbanken at approximately 50 m depth (Loeng, 1991). The topography of the sea floor influences the behaviour of the currents heavily. Dense water forms below the sea ice as the ice forms and brine is rejected resulting in water sinking to the seafloor feeding the bottom water (Midttun, 1985). Dense bottom water flows westwards through the Bjørnøyrenna channel into the Norwegian and Greenland Sea but most dense bottom water flows out of the Barents Sea between Svalbard and Frantz Josef Land into the Polar Basin (Steinsund *et al.,* 1994). Sea ice forms in the eastern and northern parts of the Barents Sea during the fall and winter and extends south to 74°N, West of 30°E and to 71°N at 35°E (Midttun, 1985).

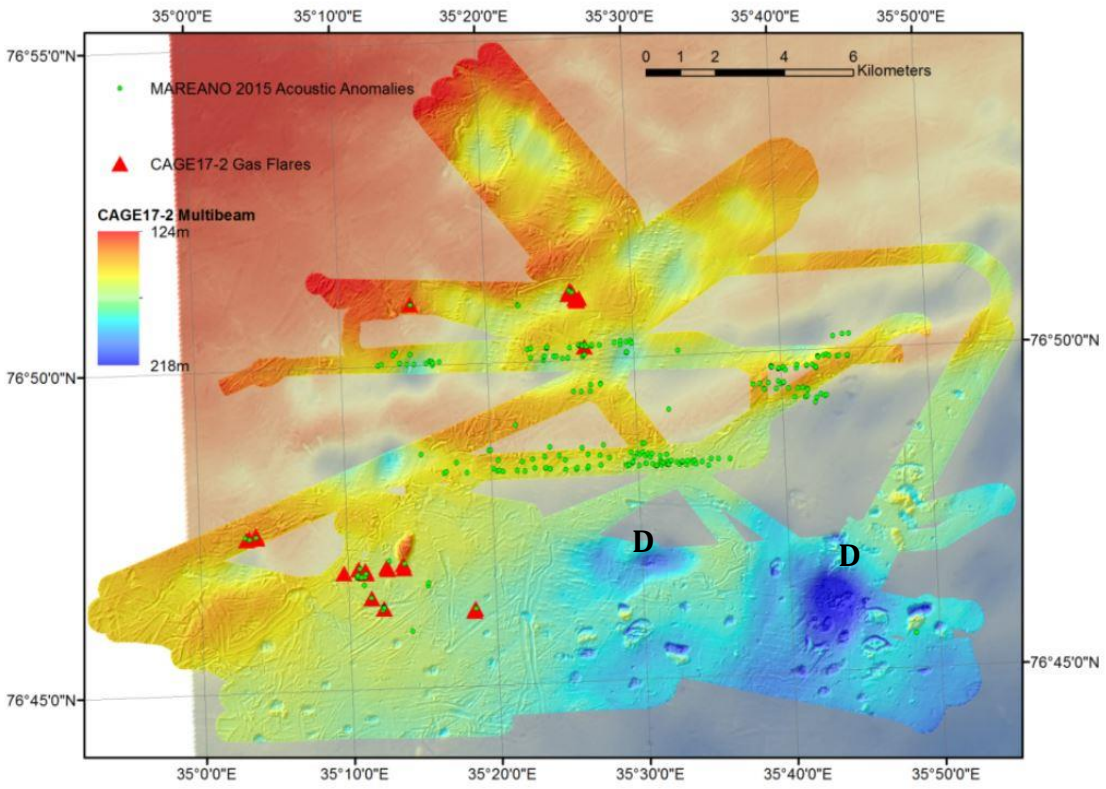

Figure 2: Gas flares locations (red triangles) observed during the CAGE 17-2 (CAGE 17-2 AMGG cruise report 2017).

1.4 Glacial and regional setting

The Barents Sea has been through many glaciations during the late Cenozoic, the most recent glacial period was the Late Weichselian (Vorren *et al*., 1988). This resulted in the Barents Sea Ice Sheet (BSIS) reaching the continental shelf break and depositing sediments on the continental slopes to form trough mouth fans (TMF) (Dowdeswell *et al.*, 1996). During this time, the whole Barents Sea continental shelf was glaciated by the Barents Sea Ice Sheet, characterized by multiple domes (Winsborrow *et al.*, 2010). These domes have been studied by Lambeck (1995) and Auriac *et al.* (2016) where they indicated that one dome is located on Storbanken, which may have stretched over Sentralbanken. Ice sheets in the Western Barents Sea extended to the outer shelf break in Bjørnøyrenna between 21.5-18.1 calibrated years before present (cal ka BP) and once before 26.5 cal ka BP (Vorren *et al.,* 1988; Svendsen *et al.,* 2004). The ice stream flowing though Bjørnøyrenna was the main conduit for the ice sheets during the Last Glacial

Maximum (LGM) (Rasmussen *et al.*, 2007). The Bjørnøyrenna Ice Stream was the largest and most powerful during deglaciation, resulting in sediment and melt water being deposited into the North Atlantic contributing to the formation of the Bjørnøya Trough Mouth Fan (Winsborrow *et al.*, 2010). During peak glacial extent the ice streams were not constrained by topography but towards the end of deglaciation, ice sheets thinned and flowed with the topography (Esteves *et al.*, 2017). Deglaciation in the Western Barents Sea had already started by 17.5 cal ka BP, which led to the Barents Sea being relatively deglaciated by 12 cal ka BP (Landvik *et al.*, 1998) (Fig. 3).

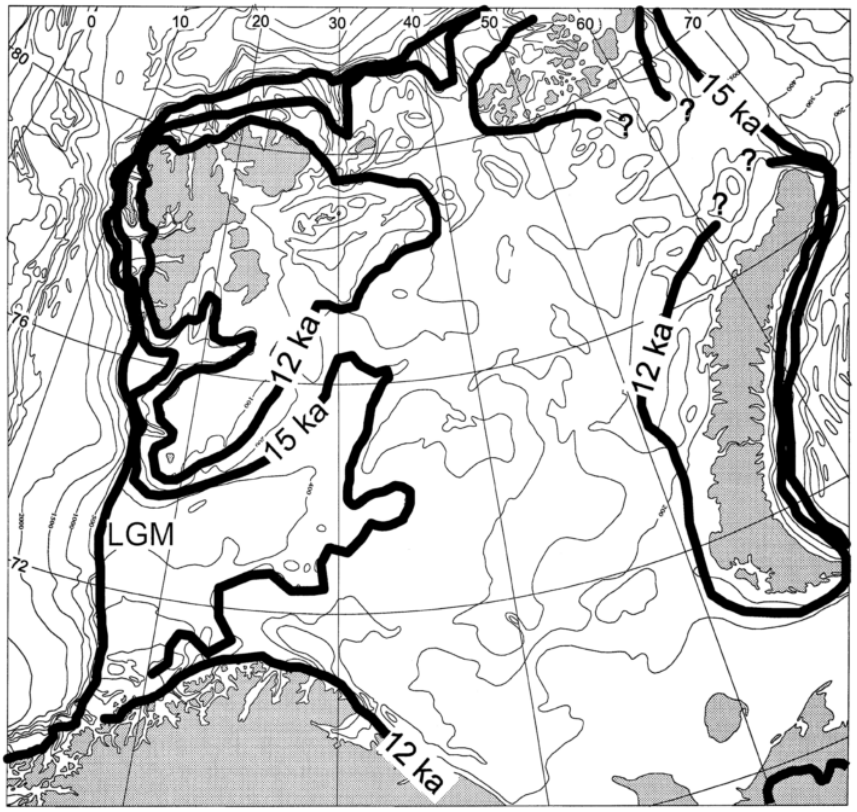

Figure 3: Ice sheet extent in the Barents Sea and deglaciation ages (Landvik et al., 1998).

1.5 The use of proxies

In this investigation, several proxies from the gravity cores were used to aid in the paleoenvironment reconstruction of the Olga Basin in the Barents Sea. A proxy is defined as a preserved physical characteristic of the environment that can stand in for direct measurements by the National Centers for Environmental Information (National Centers for Environmental Information (NCEI)). The proxies in question

are benthic foraminifera, stable isotopes of oxygen and carbon measured on planktonic foraminiferal test, organic compounds and chemical compounds of sediment.

1.5.1 Benthic Foraminifera

Foraminifera are marine based single-celled micro-organisms that have two ways of life, planktonic and benthic. Planktonic species are the minority and are found floating in the water column. Benthic foraminifera form the majority and include epifaunal and infaunal species. Epifaunal species live on the surface of a submerged substrate and infaunal species live within the sediment. Foraminifera form tests or shells commonly made of calcium carbonate ($CaCO_3$) using elements from the water column or agglutinated materials. Agglutination refers to the construction of tests by integrating exogeneous minerals into a calcareous or organic cement (Bosak *et al.*, 2011). Benthic foraminifera are usually well preserved and can be abundant in small sediment samples. Most species display a certain level of sensitivity to fluctuating environmental conditions such as water temperature, salinity and water currents (Murray, 2006). These changes are recorded during the formation of their tests as they use the elements in their surrounding at the time they existed making them great indicators of paleoenvironment (Mamo *et al.,* 2013). When the foraminiferal distribution is recorded it is possible to see how the environment changed through time. Other environmental factors that influence foraminiferal productivity include quality of organic matter for food, oxygen, light and sedimentation rates (Mamo *et al.,* 2013).

1.5.2 Stable Isotopes of oxygen and carbon in *Neogloboquadrina pachyderma*

Stable isotopes are non-radioactive atoms of the same element with the same number of protons forming the atomic number but different number of neutrons. Their chemical properties are the same due to the electronic configuration but physical properties are different. Foraminifera build their tests or shells from $CaCO_3$ therefore during their formation the isotopic ratio of Carbon (C), Calcium (Ca) and Oxygen (O) are preserved. By analysing the ratio between $^{18}O/^{16}O$ and $^{13}C/^{12}C$ the temperature and salinity of paleoenvironments can be recorded. Oxygen isotopes include ^{16}O, ^{17}O and ^{18}O, ^{16}O is the lightest form and ^{18}O is the heaviest form. When water molecules are being formed the lightest isotope ^{16}O takes less energy to be evaporated than ^{18}O, therefore during cold temperatures $\delta^{18}O$ which represents the ratio between $^{18}O/^{16}O$ will be high as the light ^{16}O would have been evaporated and trapped in ice (Fig. 4) (Columbia University). Since the ocean waters have high $\delta^{18}O$, this gets recorded in the foraminifera tests which uses the sea water to form and can be measured by an isotope ratio mass spectrometer.

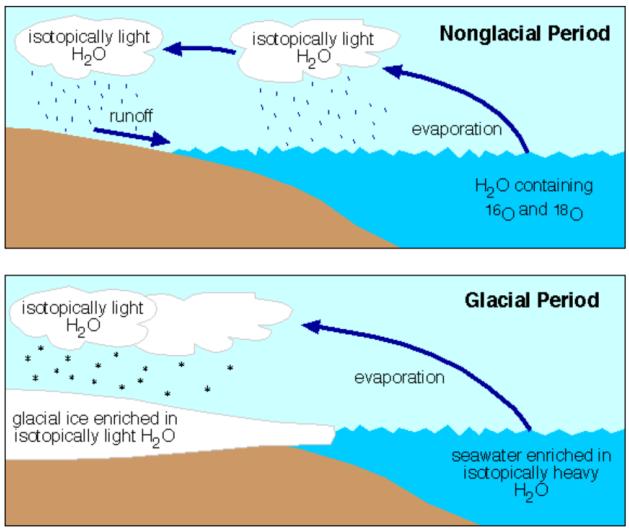

Figure 4: Nonglacial period shows light ^{16}O being evaporated and entering back into the ocean while in glacial periods this isotopically light H_2O is trapped in ice leaving the ocean enriched with heavy ^{18}O (Columbia University).

Stable isotopes of carbon include the lighter ^{12}C and heavier ^{13}C. Photosynthetic organisms prefer to use the lighter ^{12}C, thus during high primary production ^{12}C is locked away in living organisms and buried organic matter. This results in the atmosphere and ocean being enriched in ^{13}C and depleted in ^{12}C which produces high $\delta^{13}C$ ($^{13}C/^{12}C$) values. This gets reflected in the tests of foraminifera which uses the enriched ^{13}C water and indicates if the environment was suitable for biological productivity (Fig 5) (Columbia University).

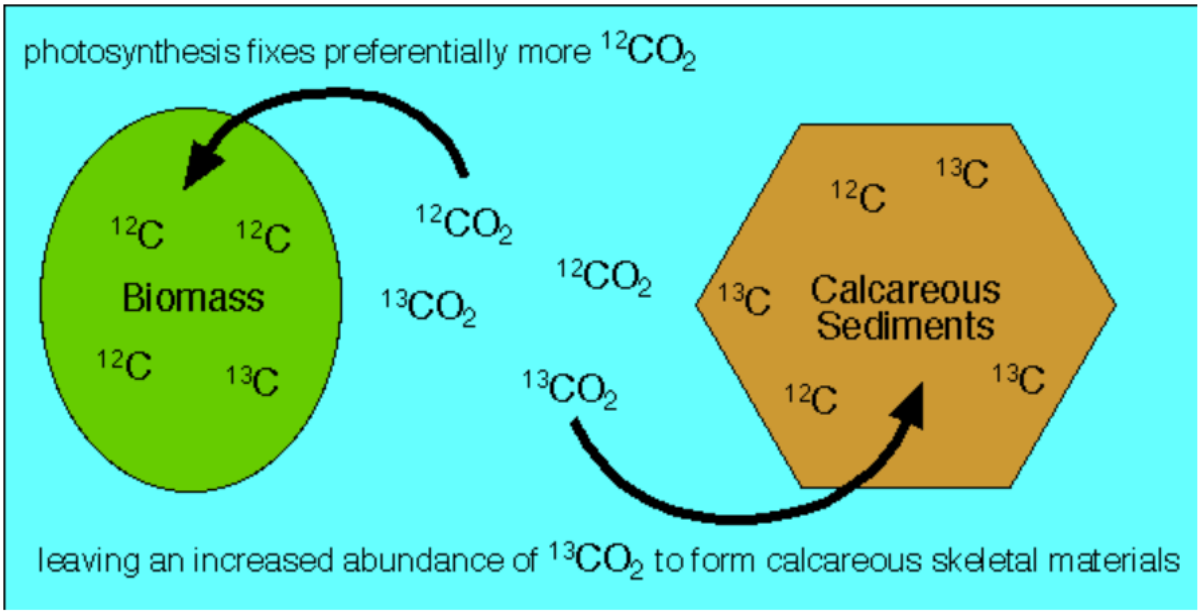

Figure 5: Simple illustration showing living organism utilising ^{12}C for photosynthesis resulting in ocean water being enriched with ^{13}C which is absorbed in the sediments, and tests and shells of micro and macrofauna (Columbia University).

1.5.3 Organic Compounds of carbon and nitrogen

The stable isotopes of organic carbon and nitrogen are commonly used as proxies for interpreting biogeochemistry or to differentiate between marine and terrestrial organic matter (Freudenthal *et al.*, 2001; Ogrinc *et al.*, 2005). Carbon is present in all organic material and as mentioned above has two stable isotopes ^{13}C and ^{12}C. $\delta^{13}C$ in this proxy is established from the sediment below the Barents Sea unlike the previous proxy where it was recorded in the tests of foraminifera and is measured as:

$$\delta^{13}C_{org}\,(‰) = [(^{13}C/^{12}C_{organic}/^{13}C/^{12}C_{V\text{–}PDB\text{–}Std}) - 1] \text{ X } 1000)$$

The cycle works the same way but instead, the high productive periods locks ^{12}C out of the sediment being buried, thus resulting in high $\delta^{13}C$ values (Fig.5). For example, sea ice cover slows down biological productivity which will result in more ^{12}C in the system and in sediments, lowering the $\delta^{13}C$ values. Nitrogen is an important nutrient element in the marine setting and its measurements provide an understanding of the past and present marine nitrogen cycle (Tesdal *et al.* 2013).

$$\delta^{15}N(‰) = [(^{15}N/^{14}N_{sample}/^{15}N/^{14}N_{atm,\ N2}) - 1] \text{ X } 1000)$$

^{15}N and ^{14}N are the two stable isotopes of nitrogen, their ratio $^{15}N/^{14}N$ is used in the equation above and represents $\delta^{15}N$. The nutrients that are used and produced by phytoplankton controls the nitrogen cycle. Phytoplankton is high quality organic matter which is further degraded after it reaches the seafloor. Therefore, it is possible to use δ15N as a proxy for nutrient utilization relating to productivity and degradation of phytodetritus (Owens, 1985).

1.5.4 Chemical compound of sediments

The chemical compound of sediments via X-ray fluorescence (XRF) is a very useful proxy as it is a non-destructive method to analyse the elemental composition of the sediments. Single element intensities are recorded which are then used as ratios and explained in the methods section. Using literature certain elemental ratio were chosen that indicate grain size, organic matter fluxes and, marine and terrigenous influences to aid in determining key climatic events.

2. Material and methods

2.1. Gravity cores

During the CAGE 17-2 AMGG cruise, three gravity cores were collected from the northern flank of the Olga Basin. The first gravity core was extracted at the centre of depression D2 and was assigned the number HH935 (Fig. 1b). Two other gravity cores were taken from the southern rim of depression D1 (HH971) and from within depression D1 (HH972). Details of the cores are given in Table 2.

Core ID	Date dd/mm/yy	Time (UTC)	Location	Co-ordinates	Length (cm)	Depth (m)
HH 935	26/06/17	22:24	Centre of D2	76°46, 84' N (Lat) 35°30, 91' E (Lon)	127	191
HH 971	30/06/17	12:47	Southern rim of D1	76°45, 86' N (Lat) 35°43, 02' E (Lon)	180	203
HH 972	30/06/17	13:46	Inside D1	76°45, 85' N (Lat) 35°43, 03' E (Lon)	215	203

Table 2: Information on sampling stations

The gravity corer used in this cruise resides on the R/V Helmer Hanssen and is made up of a 6 m long steel barrel with weights on top. The barrel has an inner diameter of 11 cm without a plastic liner which is inserted into the barrel making the inner diameter 10 cm. A core catcher and core cutter is placed on the end of the gravity core to keep sediment from falling out and aid in penetration respectively (CAGE 17-2 AMGG cruise report 2017). The gravity core is also connected to a winch, which has a wire length of 2900 m. To begin sediment core extraction, the gravity core which lies horizontally on rails is lifted vertically and lowered through R/V and into the water column using the winch until it is 20 m from the seabed. When the location for extraction is reached the gravity core is dropped, and due to gravity and the 1.6 tons weight on top, the core is pushed into the sediment. The gravity core is then lifted and brought back to deck where

the core catcher which prevented sediment from being lost on retrieval is sampled first along with the core cutter. The plastic liner is then removed, cleaned, cut into 1 m sections and labelled accordingly (CAGE 17-2 AMGG cruise report 2017).

2.2. Micropaleontological investigations

Sediment samples of 1 cm were taken from the three-sliced gravity cores every 5 cm. These 1 cm thick portions had a volume of 39.27 cm^3. The wet sediment samples were weighed and freeze dried. This process removes the water content of the sediment; thus, the dry weight was recorded so water content can be established. For micropaleontological investigation, samples were wet sieved over 100 µm mesh sieve, filtered and dried at 40°C over night. Dried samples were weighed and curated. The initial objective was to select 20 individuals of *Neogloboquadrina pachyderma*, a planktonic foraminiferal species, from each sample to undergo isotopic analysis (described in detail below). This involved dusting each sample onto a counting tray and using a binocular microscope (Leica MZ12 X1.25) to search for and identify the correct genus and species of planktonic foraminifera. Once the *N. pachyderma* were located, they were picked and placed in separate slides with a label corresponding to the core, horizon and sieving size. It soon became clear that most samples did not contain enough individuals to go through efficient isotopic analysis, hence, only 25 samples were used from the 96 samples that were available from all 3 cores. The next step in the foraminiferal investigation was to identify the most abundant benthic foraminiferal species in order to plot their distribution and use their trend to reconstruct the paleoenvironment. The aim was to pick and identify, when it was possible, a minimum of 250 benthic foraminiferal specimens from samples at 10 cm intervals. Different species were all mixed into one slide after initial selection, species identification took place and the foraminifera were sorted, counted and documented onto numbered grid slides. For many samples that number could not

be reached and all benthic foraminifera were supposedly picked. When the number of foraminifera were very low in several successive intervals, intermediate intervals were investigated to get significant numbers. For example, intervals 70-71 cm and 80-81 cm only contained 10 individuals of 3 species and 4 individuals of 2 species respectively leading to investigations of interval 75-76 cm. To plot the foraminiferal distribution, the relative abundance of each species was calculated as a percentage from the total count of the sample, as following:

$$\frac{Number\ of\ specific\ species}{Total\ number\ of\ benthic\ foraminifera} \times 100 = Species\ relative\ abundance\ (\%)$$

The Shannon index (H) was used to determine species diversity along the core with the Evenness index (E) to determine how the species are equilibrated in the samples distribution using the PAST software.

2.3. Stable isotope analysis

Neogloboquadrina pachyderma specimens were chosen to perform isotopic analysis due to their dominance in the Arctic Ocean as a planktonic species (Carstens and Wefer, 1992). Being the dominant planktonic species in the Arctic, isotopic data are usually measured on *N. pachyderma* (e.g., Bauch, Carstens and Wefer, 1997) which makes comparing data easier. The specimens collected in the slides during picking were carefully transferred to small glass vials (Fig. 6), making sure all the foraminifera sat at the bottom of the vial so the phosphoric acid could reach it. Vials were marked with numbers corresponding to their interval in the cores and then analysed in the Stable Isotope Laboratory (SIL) at CAGE, Centre for Arctic Gas Hydrate, Environment and Climate in the Department of Geosciences at The Arctic University of Norway in Tromsø (UiT, Tromsø). The equipment used in this analysis was the Thermo-Fisher MAT253 IRMS with a Gasbench II which is

used to read $\delta^{13}C$ and $\delta^{18}O$ concentrations in carbonates. The Gasbench II is first used to create CO_2 from the carbonate tests of the specimens.

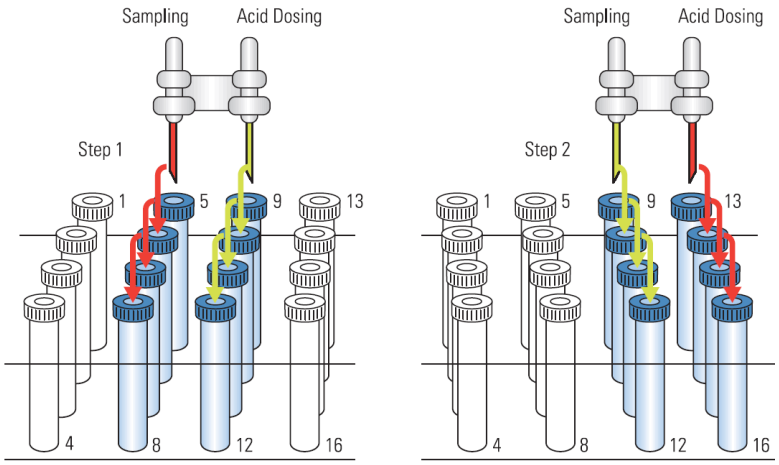

Figure 6: The Carbonate Reaction Kit (Thermo Scientific GasBench II Brochure)

This is done by the dissolution of the foraminiferal tests, a process called 'acid bath' and involves a microliter pump, injecting phosphoric acid into the sample vials shown in Figure 6 and produces precision of 0.08 ‰ for $\delta^{18}O$ and of 0.06 ‰ for $\delta^{13}C$ (Thermo Scientific GasBench II Brochure). The phosphoric acid (H_3PO_4) causes dissolution of the calcium carbonate ($CaCO_3$) which is the material that forms the tests of foraminifera resulting in a gas composed of calcium phosphate ($CaHPO_4$), water (H_2O) and carbon dioxide (CO_2) to be released shown in the equation below.

$$CaCO_3 + H_3PO_4 = CO_2 + H_2O + CaHPO_4$$

The gas in the vial is then diluted with helium (He) which displaces it allowing an upward flow out of the vial and into a diffusion trap where water is removed. The gas then flows through a loop which aliquots the sample onto the gas chromatograph (GC) column, separating the molecules (Thermo Scientific GasBench II Brochure). A reference gas is injected which allows accurate

referencing of the sample to isotopic standards and the remaining separated particles is sent to the isotope ratio mass spectrometry (IRMS) (Fig. 7).

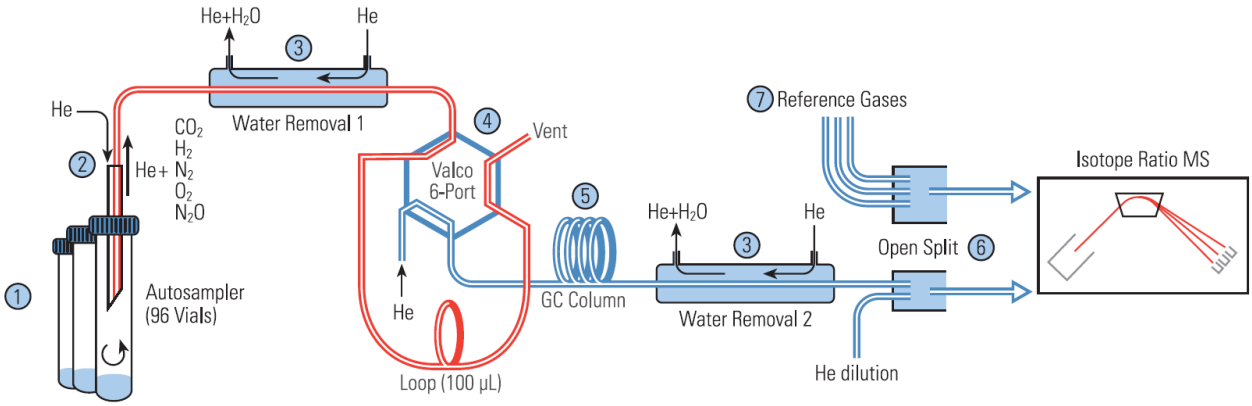

Figure 7: Gasbench Scheme (Thermo Scientific GasBench II Brochure)

The carbon or oxygen particles enters the Thermo-Fisher MAT253 IRMS and gets ionized by an ion source creating a positive charge which are then propelled forward by an electric field. The particles then reach a magnetic field where the path of propulsion is deflected depending on its mass, heavy particles deflect less while lighter particles deflect more (Fig. 8). This process separates elements of different masses (Isotopes) such as carbon (C) to ^{12}C, ^{13}C and ^{15}C and oxygen (O) to ^{16}O and ^{18}O.

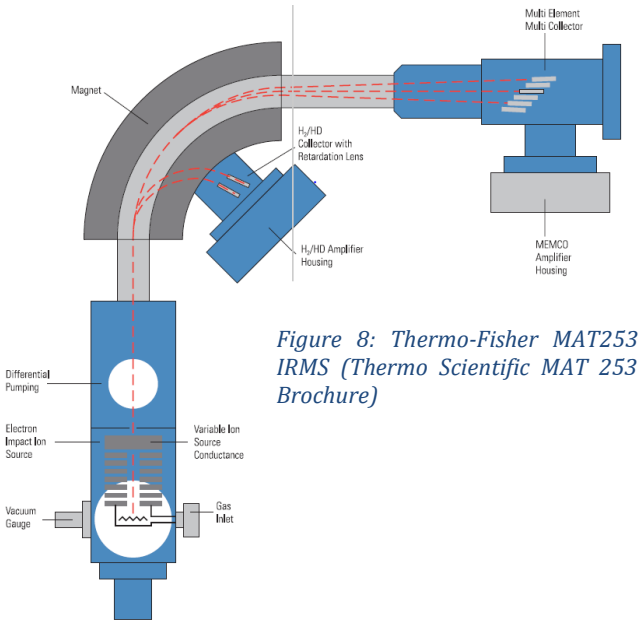

Figure 8: Thermo-Fisher MAT253 IRMS (Thermo Scientific MAT 253 Brochure)

The particles then hit a detector plate where the abundance of an isotope is measured. In this study, ^{13}C and ^{18}O isotopes were measured from the tests of *N. pachyderma* and used as indicators for paleoclimate. Figure 8 shows the inner workings of the Thermo-Fisher MAT253 IRMS (Thermo Scientific MAT 253 Brochure).

2.4. Organic compounds analysis

During the early stages of core sampling, the technical staff at SIL proceeded with analysing the organic compounds of the samples. After the 1 cm samples were taken at 5 cm intervals and freeze-dried, 0.5 g were removed from each sample and treated with hydrochloric acid for 4-8 hours, which removed the carbonates and released CO_2. The acid was then washed away and samples are dried. 10 mg were taken from the remaining organic material and placed in tin capsules which were introduced to the combustion reactor of the Thermo Scientific FLASH 2000 HT Elemental Analyzer with the proper amount of oxygen (Thermo Fisher brochure). The sample was then burned at 1020^{o}C and the resultant gases were carried by a helium flow into a reactor where carbon is converted to CO_2 and nitrogen is converted to N_2. These gases then went through a water trap removing H_2O followed by a GC column separating the carbon and nitrogen which can be fed into the IRMS (Fig. 4). The IRMS analysed the individual particles against the Vienna Pee Dee Belemnite (VPDB) for carbon and relative air for nitrogen and produced the abundance of ^{13}C and ^{15}N isotopes through the process described above (Fig. 9).

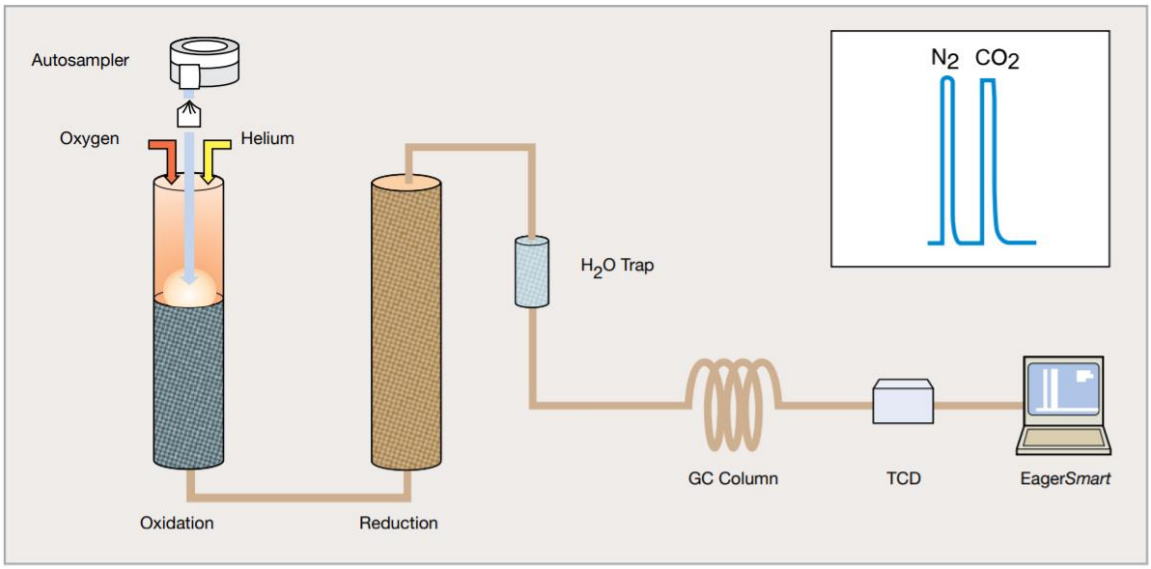

Figure 9: Flash 2000 elemental analyser process (Thermo Fisher Brochure)

2.5. X-ray fluorescence (XRF) analysis

Gravity cores HH935, 971 and 972 were split in length in the laboratory at the Department of Geosciences at UiT and were scanned by an Avaatech XRF core scanner. The XRF core scanner can scan a one-meter long core section with a resolution of 1 cm in 30 minutes and gives us an estimation of the elemental composition of the sediment. Scanning involves bombarding the sediment with high energy X-rays from a source, this ionizes the atoms resulting in an electron from the inner shell being kicked out. Almost immediately an electron from the outer shells falls in and takes its place emitting radiation which is then picked up by a detector. Each element has its own characteristic energy therefore using the radiation that has been emitted, it is possible to measure the elemental composition of sediment samples. Elemental ratios have been utilized as environmental indicators instead of single element intensities as they are suitable for correlation and have been used by several authors, such as (Rothwell *et al.,* 2006; Calvert *et al.,* 2007; Lucchi *et al.*, 2013). Ratios of two elements also reduce the effects of down core variations (Weltje *et al.,* 2008). The XRF scanning method can measure Ca (Calcium), Fe (Iron) and Ti (Titanium) reliably which have been

used in this study along with Zr (Zirconium), Rb (Rubidium), Br (Bromine) and Cl (Chlorine). Ti and Ca have been applied into many studies to deduce terrigenous and marine constituents, Ti is constrained to lithogenic sediments and is resistant to diagenetic processes (Stuut *et al.* 2014) and Ca measures the biogenic carbonate abundance. Using the Ca/Ti ratio as a proxy it is possible to track the changes in biogenic and lithogenic sedimentation (Rothwell *et al.,* 2015). Fe is also used when detailing terrigenous sediment delivery and is an indicator for climatic changes on the continent. The Fe/Ca ratio is used to measure the relative proportions of terrigenous fluxes against marine carbonate (Adegbie *et al.*, 2003). The Zr/Rb ratio is a well-known proxy for grain size since Zr exist in coarser particles than Rb (Schneider *et al.*, 1997) and the Br/Cl ratio was used as a proxy for organic matter by Thomson *et al.* (2006).

2.6. Radiocarbon dating

In order to date specific intervals in the cores, bivalve shell fragments from selected samples were sent to the Beta Analytic testing laboratory. This first involved choosing the depths which would most benefit from ageing. Two samples were chosen at 45-46 and at 95-96 cm from core HH972. The interval 45-46 cm is in a zone with a noticeable shift in the $\delta^{13}C$ of *N. pachyderma,* which deserves a closer look and at 95-96 cm there is a transition in the organic compounds of $\delta^{13}C$ and $\delta^{15}N$ in HH972. Calcite shell fragments of bivalve were then picked from the selected samples. Fragments from 95-96 cm interval were chosen directly at the depth of the irregularity while the 45-46 cm interval was chosen because it presented a significant number of fragments to undergo dating and provide a little age model. Fragments were picked using the same method as in the micropaleontological investigation and kept in slides which were later weighed, details of these samples can be found in Table 4.

Core ID	Interval (cm)	Sample mass (mg)	Non-calibrated age (BP)	Age calendar (BP)	Analytical error (±)	Material used (Marine)
HH972	45-46	3.75	4990	5420	30	Shell
	95-96	3.92	9310	9730	40	Shell

Table 3: Radiocarbon dating results

The samples underwent Accelerator Mass Spectrometry (AMS) dating which is indicative of samples weighing between 5-100 mg. Before the process of dating begins, the samples were washed with deionized water which removes the debris. The material was then crushed and subjected to hydrochloric acid (HCl) etches to remove 10-30% of the total weight, which leaves only the primary carbonate. The cleaned samples were then subjected to immense heat, which converts the carbonate to CO_2 and leads to graphitization with a metal catalyst, this is a two-stage reaction as shown below (Beta Analytic Methodology).

The first reaction- water-gas shift reaction: reduction to carbon monoxide

$$CO_2 + H_2 \rightarrow CO + H_2O$$

The second reaction controls the overall reaction rate: reduction to carbon

$$CO + H_2 \rightarrow C + H_2O$$

The few milligrams of graphite are pressed onto a metal disc along with reference materials and used in the AMS. The AMS propels ions at high kinetic energies at the disc producing negatively charged ionized carbon atoms, which pass through focussing fields and eventually become positively charged atoms due to a gas or metal foil resulting in loss of electrons. These carbon atoms go through further

focusing and head to towards the mass analysis which is where a magnetic field deflects these particles, the degree of deflection depends on the mass similar to the IRMS process and the ^{14}C as well as the ^{12}C and ^{13}C are counted on a detector (Beta Analytic Methodology). Dating is then completed by measuring the ratio of ^{14}C to ^{12}C and by using the half-life of ^{14}C which is 5,730 years therefore generally works for aging up to 60,000 years old. The results were calibrated by BetaCal3.21: HPD method: MARINE13 and the dating standard used was 'Before Present' (BP).

3. Results

3.1. Foraminiferal distribution

Thirty-four different benthic foraminiferal species were identified from 28 samples at 10 cm intervals in cores HH935, HH971 and HH972. Only the species with a percentage >5% have been included in this analysis. A total of 35 species, mainly calcareous and only one agglutinated (*Recurvoides turbinatus*) were discovered. Calculated total numbers of benthic foraminifera are presented in Table 5. The most abundant species in the benthic foraminiferal assemblages are: *Melonis barleeanus, Cibicidoides lobatulus, Elphidium excavatum, Astrononion gallowayi, Cassidulina reniforme, Cassidulina neoteretis, Islandiella norcrossi, Buccella frigida and Recurvoides turbinatus* (Table 4). No species were observed to truly dominate an assemblage. The plots below show that all three cores were devoid of foraminifera below approximately 80-90 cm bsf (below seafloor). HH935 and HH971 both show decreasing trends in foraminiferal density (Fig. 10a, b) towards this change while HH972 does not show the same trend (Fig. 10c). The 20 cm interval bsf of HH935 contains 155 individual specimens (Table 5a) making it the most concentrated layer (197.35 ind. 50 cm^3) (Fig. 10a) followed by the 40 cm interval containing 117 individuals (148.97 ind. 50 cm^3) (Fig. 10a), below this, density is drastically reduced. 50 cm^3 is used as a round number for the foraminiferal density since the original volume is 39.27 cm^3, the individual number

has been converted accordingly. HH971 shows a strong decreasing trend from 468.55 ind. 50 cm^3 in the first interval to 3.82 ind. 50 cm^3 (Fig. 10b). HH972 has an even density throughout the core at roughly 140 ind. 50 cm^3. Unlike the others the densest interval occurs at a lower depth of 90 cm (236.82 ind. 50 cm^3) (Fig. 10c). The specific richness (S) follows a similar trend to the foraminiferal density. S generally illustrates a decreasing trend in HH935 and HH971 (Fig. 10a, b) and stays even with depth in HH972 (Fig. 10c). The biodiversity indices, Shannon index (H') and Evenness index (E) show fairly different trends in each core. H' is high in the first 40 cm bsf of HH935 then drops to 0 at 80 cm bsf (Fig. 10a). E falls to a low of 0.55 at 20 cm bsf then fluctuates as it increases to 1 at 80 cm bsf (Fig 10 a), H' and E have loosely similar trends. H' in HH971 stays at 2 to a depth of 60 cm where there is a rapid decrease and increase, E on the other hand fluctuates roughly between 0.8 and 0.9 throughout the core (Fig. 10b). HH972 show matching trends in H' and E with a slight decrease from the surface and a trough at 60 cm bsf (Fig. 10c). Figure 11 illustrates the individual specimens count produced from Table 5 and Table 6 shows the relative abundances of major species used to produce Figure 12.

Accepted species names according to The World Register of Marine Species (WoRMS)	**References**	**Species names used in this study**	**References**
Melonis barleeanus	(Williamson, 1858)	*Melonis barleeanus*	(Williamson, 1858)
Cibicidoides lobatulus	(Walker & Jacob, 1878)	*Cibicidoides lobatulus*	(Walker & Jacob, 1878)
Cribroelphidium excavatum	(Terquem, 1875)	*Elphidium excavatum*	(Terquem, 1875)
Astrononion hamadaense	(Asano, 1950)	Astrononion gallowayi	Loeblich & Tappan, 1953
Cassidulina reniforme	(Nørvang, 1945)	*Cassidulina reniforme*	(Nørvang, 1945)
Cassidulina neoteretis	(Seidenkrantz, 1995)	*Cassidulina neoteretis*	(Seidenkrantz, 1995)
Islandiella norcrossi	(Cushman, 1933)	*Islandiella norcrossi*	(Cushman, 1933)
Buccella frigida	(Cushman, 1922)	*Buccella frigida*	(Cushman, 1922)
Recurvoides turbinatus	(Brady, 1881)	*Recurvoides turbinatus*	(Brady, 1881)

Table 4: Major species identified in this study

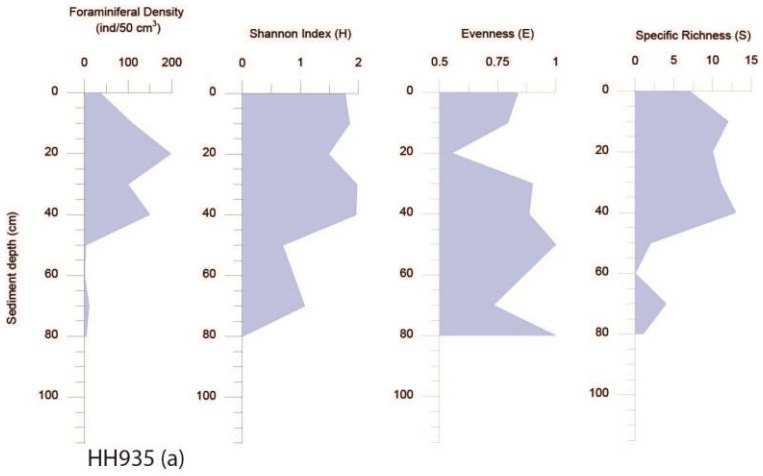

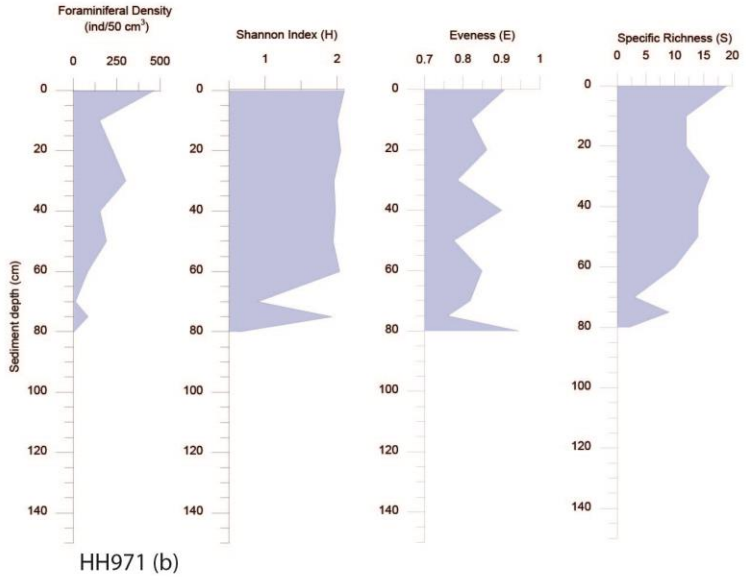

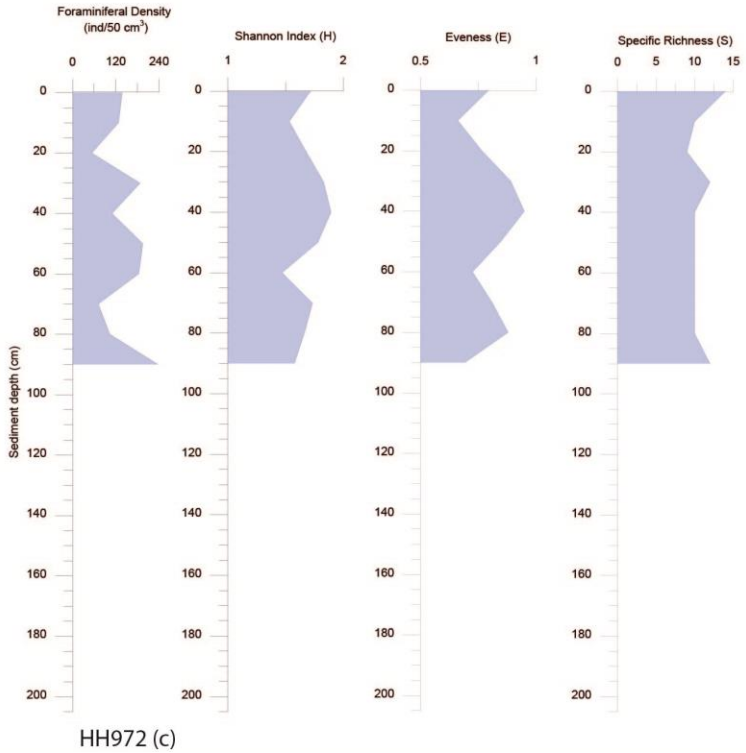

Figure 10: Foraminiferal density, Shannon index (H), Evenness index (E) and Specific richness (S) plots for cores (a) HH935, (B) HH971 and (C) HH972

3.1.1. Core HH17-2-935 GC

The benthic foraminiferal assemblage of HH935 includes seven major species, *C. neoteretis* and *R. turbinatus* were not included due to low relative abundances (Fig. 12a).

3.1.1.1. Dominant species

Although *M. barleeanus* (25%) and *B. frigida* (28.57%) are abundant in the surface sediments, it is the only interval they dominate (Fig 12a). *Astrononion gallowayi* percentages remain high at further depths along with other species. *Islandiella norcrossi* peaks at the 10 cm interval with a relative abundance of 21% and is second to *A. gallowayi* with 31%. *Astrononion gallowayi* is the prominent species up to 50 cm depth along with *E. excavatum* at the 30 and 50 cm interval. 50 cm depth only contained one of each species (Table 5a). Below 60 cm depth, only 5 species were identified. *Cibicidoides lobatulus* has a high relative abundance at 70 cm with 62% and only 3 *E. excavatum* were found at 80 cm. A significant decrease in relative abundance of *M. barleeanus* can be observed from the top interval to 20 cm depth, which coincides with a sharp decrease in *B. frigida*, furthermore, *A. gallowayi* and *I. norcrossi* show a substantial increase from the sea floor to 20 cm and 10 cm depth, respectively (Fig. 12a). *Cassidulina reniforme* and *B. frigida* are observed to have similar trends with peaks and troughs at the same depths and *E. excavatum* shows an increasing trend down to 50 cm. Relative abundances below 40 cm depth seem high due to low foraminiferal counts shown in Table 5.

3.1.2. Core HH17-2-971 GC

8 major species form the benthic foraminiferal assemblage of HH971, not including *Cibicidoides lobatulus* (Fig. 12b). *Recurvoides turbinatus* only appears as a

major species in this core. Data was collected from the intermediate interval of 75-76 cm due to lack of foraminifera in surrounding intervals.

3.1.2.1. Dominant species

Astrononion gallowayi is prevalent in first interval with 24% abundance and remains dominant to 30 cm depth. The 10 cm interval contains a foraminiferal assemblage of *E. excavatum, A. gallowayi* and *C. reniforme* making up a total abundance of 20% each. *Elphidium excavatum* and *A. gallowayi* dominate at 30 cm depth with a relative abundance of 22% each and *E. excavatum* remains abundant from 50-70 cm with *C. reniforme* also forming a significant amount from 40-60 cm. *Elphidium excavatum* has an increasing trend with two major troughs (Fig 12b). The 20 cm and 40 cm interval both show approximately 10% falls in their relative abundance. The decrease to 20 cm depth coincides with the decrease observed in *C. reniforme* to 20 cm of approximately 13% (Fig. 12b). The relative abundance of *C. reniforme* increases sharply after the fall at the 20 cm to 28% in the 40 cm interval. Relative abundance takes a gentle decrease of approximately 5% to the 60 cm interval where numbers suddenly plummet by 21% in the 75 cm interval. *Astrononion gallowayi* is observed to be the most abundant in the first 30 cm with little fluctuations. A major decrease of 15% is seen to occur at the 50 cm interval, which is where the relative abundance remains. A clear increasing with depth trend can be seen in *C. neoteretis* with some fluctuations which peak at 18% in the 75 cm interval. *Buccella frigida* and *R. turbinatus* show similar trends with a dip at the 40 cm interval and a gradual increase and decrease.

3.1.3. Core HH17-2-972 GC

HH972 includes the least number of major species, *C. lobatulus, R. turbinatus* and *C. neoteretis* all had <5% abundance (Fig. 12c).

3.1.3.1. Dominant species

Astrononion gallowayi and *I. norcrossi* have the highest relative abundance of 30% and 25%, respectively in the first interval. *Astrononion gallowayi* peaks at 10 cm depth with a relative abundance of 52% and continues to dominate from 20-40 cm. From 40 cm, a sharp decrease can be observed down to 4% at the 90 cm interval. *Elphidium excavatum* relative abundance is fairly low at shallow depths compared to 30-90 cm intervals where abundance peaks at 60 cm with 50% but still remains high. *Buccella frigida* fluctuates around 10% relative abundance but is at its highest at 50 cm depth with approximately 23% coinciding with the peak of *C. reniforme* at 25% (Fig. 12c). *Melonis barleeanus* barely has a presence in the first interval but fluctuates around 10% from 10-70 cm and peaks at 80 cm depth with a relative abundance of approximately 25%. *Elphidium excavatum* has a roughly increasing trend with two major peaks at 60 and 90 cm with 50% and 45% respectively, on the other hand *A. gallowayi* shows a strong decreasing trend.

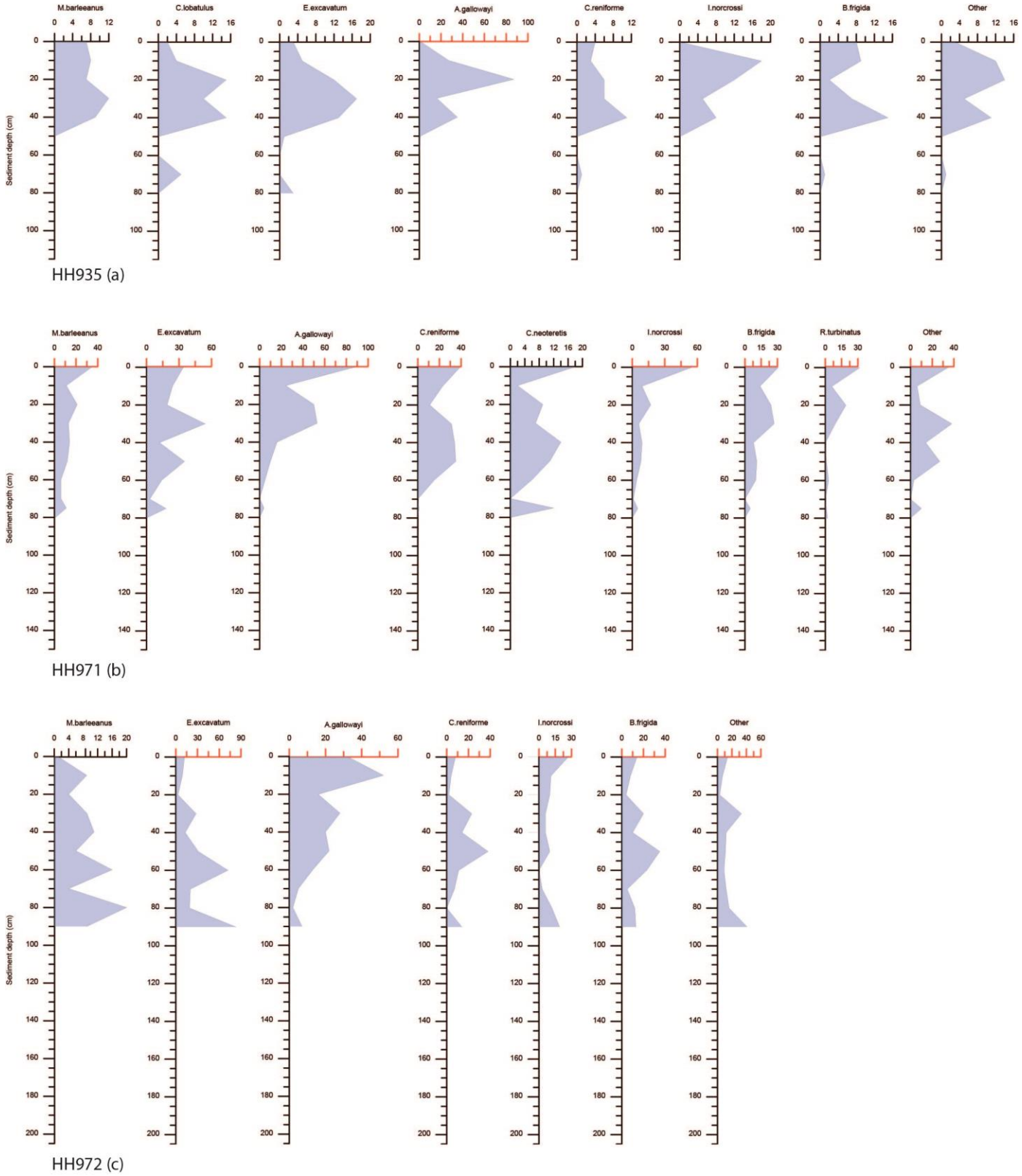

Figure 11: Individual specimens count of major species (a) HH935, (b) HH971, (c) HH972. Red x-axis illustrates a different scale

HH935 (a)

Depth (cm)	M.barleeanus	C.lobatulus	E.excavatum	A.gallowayi	C.reniforme	I.norcrossi	B.frigida	Other	Total ind.	S. richness (Total 18)
0-1	7	2	3	1	4	0	8	3	28	7
10-11	8	4	5	27	3	18	9	12	86	12
20-21	7	15	12	87	6	12	2	14	155	10
30-31	12	10	17	16	6	5	7	5	78	11
40-41	9	15	13	35	11	8	15	11	117	13
50-51	0	0	1	1	0	0	0	0	2	2
60-61	0	0	0	0	0	0	0	0	0	0
70-71	0	5	0	0	1	0	1	1	8	4
80-81	0	0	3	0	0	0	0	0	3	1
Total ind.	**43**	**51**	**54**	**167**	**31**	**43**	**42**	**46**	**477**	

HH971 (b)

Depth (cm)	M.barleeanus	E.excavatum	A.gallowayi	C.reniforme	C.neoteretis	I.norcrossi	B.frigida	R.turbinatus	Other	Total ind.	S. richness (Total 30)
0-1	35	34	89	39	18	55	31	32	35	368	19
10-11	11	24	24	23	2	9	14	6	6	119	12
20-21	21	19	50	11	9	17	24	19	9	179	12
30-31	13	54	53	31	7	6	27	9	38	238	16
40-41	14	12	16	34	14	9	8	0	14	121	14
50-51	12	35	10	35	11	8	11	1	27	150	14
60-61	6	14	5	15	6	4	10	3	3	66	10
70-71	6	3	0	0	0	1	0	0	0	10	3
75-76	11	18	4	1	12	5	5	1	10	67	9
80-81	1	0	0	0	0	0	0	2	0	3	2
Total ind.	**130**	**213**	**251**	**189**	**79**	**114**	**130**	**73**	**142**	**1321**	

HH972 (c)

Depth (cm)	M.barleeanus	E.excavatum	A.gallowayi	C.reniforme	I.norcrossi	B.frigida	Other	Total ind.	S. richness (Total 24)
0-1	1	12	32	8	27	14	14	108	14
10-11	9	9	52	4	11	8	7	100	10
20-21	4	3	16	2	10	4	3	42	9
30-31	9	28	28	23	6	20	33	147	12
40-41	11	13	20	14	6	10	12	86	10
50-51	6	31	22	38	10	35	11	153	10
60-61	16	72	13	11	0	23	9	144	10
70-71	4	20	5	7	3	5	12	56	10
80-81	20	19	2	0	12	12	16	81	10
90-91	9	83	7	14	19	13	41	186	12
Total ind.	**89**	**290**	**197**	**121**	**104**	**144**	**158**	**1103**	

Table 5: Total individual foraminiferal count and specific richness (S)

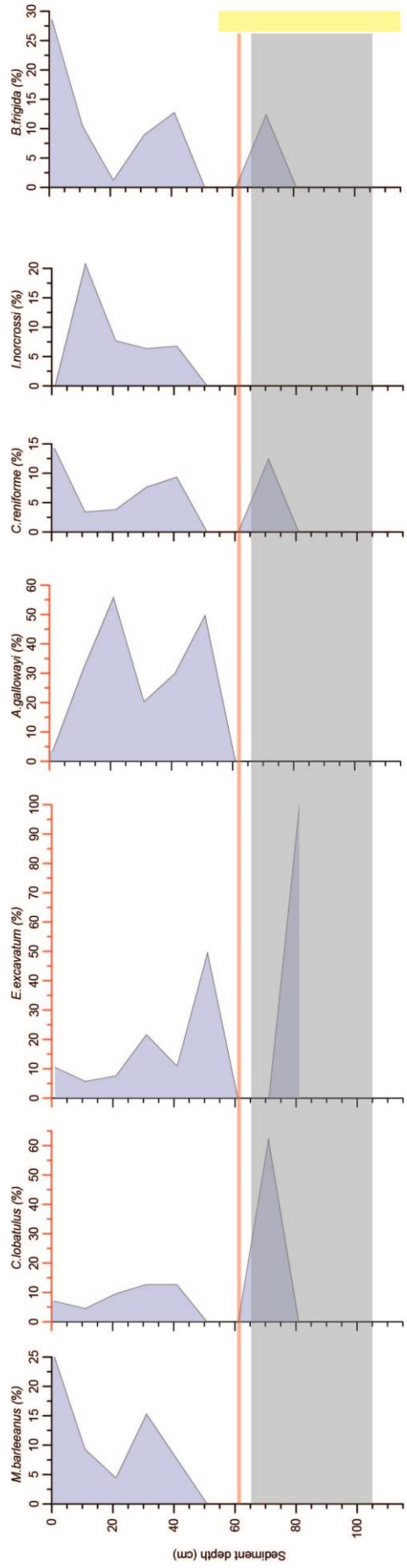

Figure 12 (a): Relative abundance of major species. Grey bar illustrates depths with IRD and yellow bar indicates the presence of pyrite. Purple line marks depths that have been aged (BP).

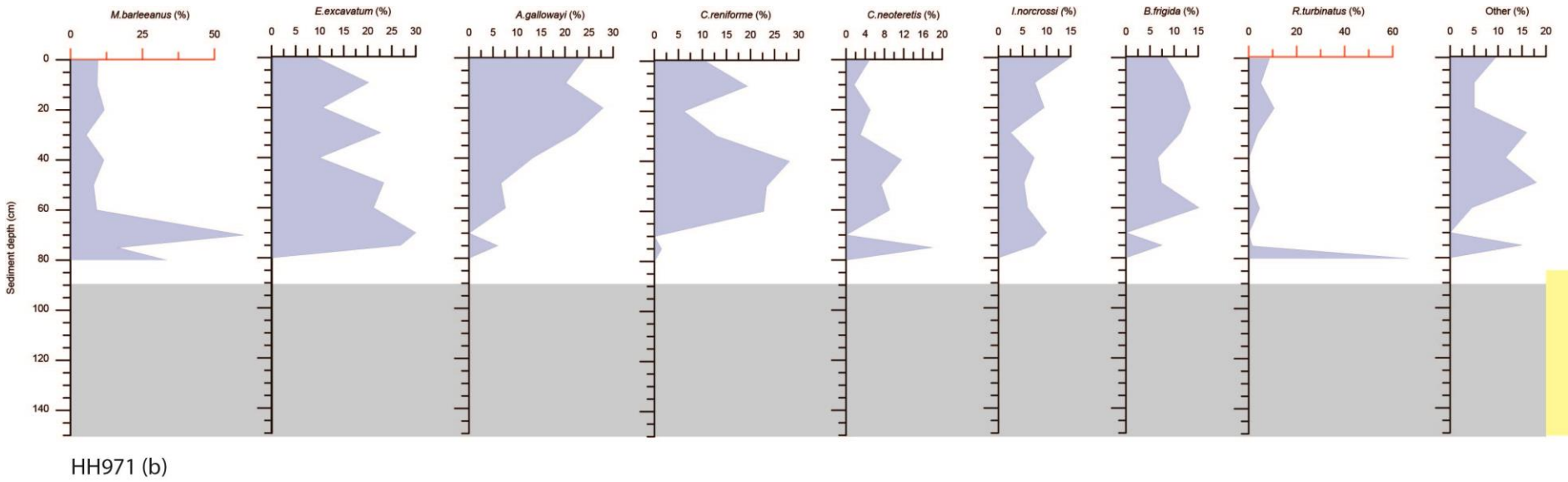

Figure 12 (b): Relative abundance of major species. Grey bar illustrates depths with IRD and yellow bar indicates the presence of pyrite. Purple line marks depths that have been aged (BP).

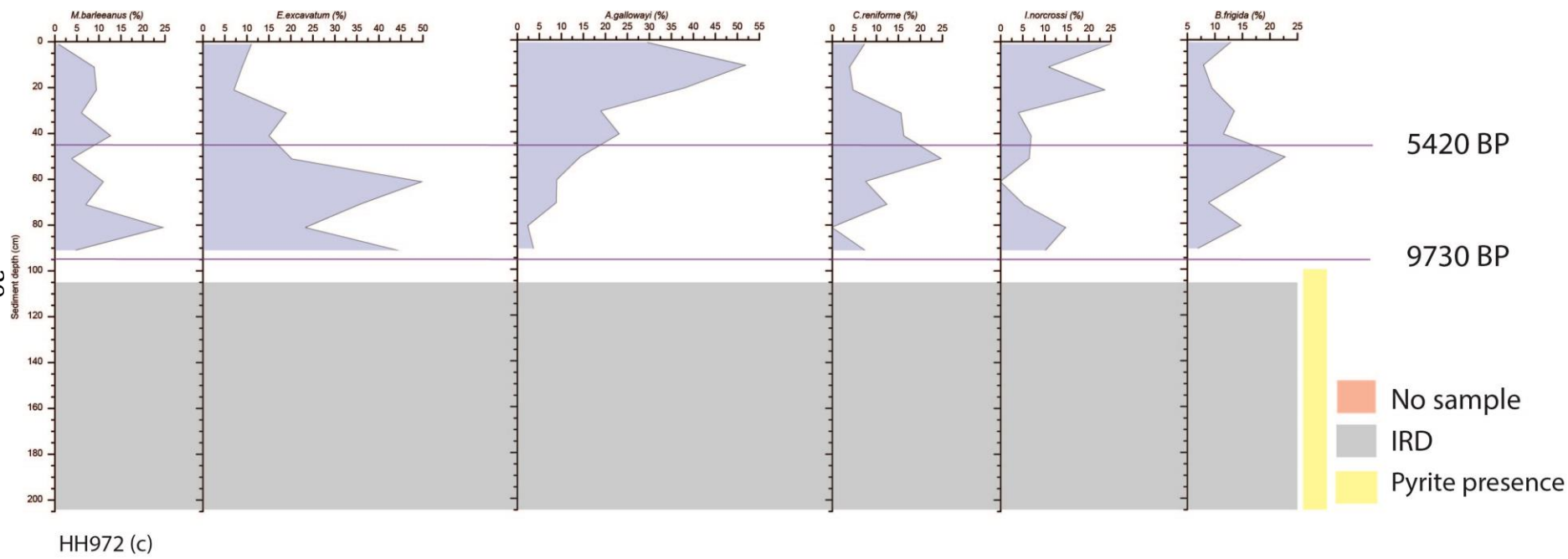

Figure 12 (c): Relative abundance of major species. Grey bar illustrates depths with IRD and yellow bar indicates the presence of pyrite. Purple line marks depths that have been aged (BP).

HH935 (a)

Depth (cm)	M.barleeanus (%)	C.lobatulus (%)	E.excavatum (%)	A.gallowayi (%)	C.reniforme (%)	I.norcrossi (%)	B.frigida (%)	Other (%)
0-1	25.00	7.14	10.71	3.57	14.29	0.00	28.57	10.71
10-11	9.30	4.65	5.81	31.40	3.49	20.93	10.47	13.95
20-21	4.52	9.68	7.74	56.13	3.87	7.74	1.29	9.03
30-31	15.38	12.82	21.79	20.51	7.69	6.41	8.97	6.41
40-41	7.69	12.82	11.11	29.91	9.40	6.84	12.82	9.40
50-51	0.00	0.00	50.00	50.00	0.00	0.00	0.00	0.00
60-61	0.00	0.00	0.00	0.00	0.00	0.00	0.00	0.00
70-71	0.00	62.50	0.00	0.00	12.50	0.00	12.50	12.50
80-81	0.00	0.00	100.00	0.00	0.00	0.00	0.00	0.00

HH971 (b)

Depth (cm)	M.barleeanus (%)	E.excavatum (%)	A.gallowayi (%)	C.reniforme (%)	C.neoteretis (%)	I.norcrossi (%)	B.frigida (%)	R.turbinatus (%)	Other (%)
0-1	9.51	9.24	24.18	10.60	4.89	14.95	8.42	8.70	9.51
10-11	9.24	20.17	20.17	19.33	1.68	7.56	11.76	5.04	5.04
20-21	11.73	10.61	27.93	6.15	5.03	9.50	13.41	10.61	5.03
30-31	5.46	22.69	22.27	13.03	2.94	2.52	11.34	3.78	15.97
40-41	11.57	9.92	13.22	28.10	11.57	7.44	6.61	0.00	11.57
50-51	8.00	23.33	6.67	23.33	7.33	5.33	7.33	0.67	18.00
60-61	9.09	21.21	7.58	22.73	9.09	6.06	15.15	4.55	4.55
70-71	60.00	30.00	0.00	0.00	0.00	10.00	0.00	0.00	0.00
75-76	16.42	26.87	5.97	1.49	17.91	7.46	7.46	1.49	14.93
80-81	33.33	0.00	0.00	0.00	0.00	0.00	0.00	66.67	0.00

HH972 (c)

Depth (cm)	M.barleeanus (%)	E.excavatum (%)	A.gallowayi (%)	C.reniforme (%)	I.norcrossi (%)	B.frigida (%)	Other (%)
0-1	0.93	11.11	29.63	7.41	25.00	12.96	12.96
10-11	9.00	9.00	52.00	4.00	11.00	8.00	7.00
20-21	9.52	7.14	38.10	4.76	23.81	9.52	7.14
30-31	6.12	19.05	19.05	15.65	4.08	13.61	22.45
40-41	12.79	15.12	23.26	16.28	6.98	11.63	13.95
50-51	3.92	20.26	14.38	24.84	6.54	22.88	7.19
60-61	11.11	50.00	9.03	7.64	0.00	15.97	6.25
70-71	7.14	35.71	8.93	12.50	5.36	8.93	21.43
80-81	24.69	23.46	2.47	0.00	14.81	14.81	19.75
90-91	4.84	44.62	3.76	7.53	10.22	6.99	22.04

Table 6: Relative abundance of major species table.

3.2. Stable isotopes: Oxygen and Carbon in *Neogloboquadrina pachyderma*

25 samples underwent isotopic analysis and produced values that fluctuated above and below the average (Fig. 13). $\delta^{13}C$ values ranged from 0.38‰ to 0.69‰ and $\delta^{18}O$ values ranged from 3.97‰ to 4.16‰ in the three cores. $\delta^{13}C$ results showed significant changes of 0.2‰ to 0.3‰ unlike $\delta^{18}O$ which recorded changes of 0.14‰ or below. Samples that had appropriate amounts of *N. pachyderma* for IRMS were only found from 0-25 cm depth in HH935, this increased to 0-60 cm and 0-65 cm in HH971 and HH972 respectively therefore, below these intervals no data was collected. Top 15 cm seems to be missing in HH935 and HH971 shown by constant $\delta^{18}O$ in HH972.

3.2.1. Core HH17-2-935 GC

From 0-20 cm $\delta^{13}C$ and $\delta^{18}O$ have opposite trends with an exception at 25 cm where they both shown an increase towards the average core value of 0.48‰ ($\delta^{13}C$) and 4.03‰ ($\delta^{18}O$) (Fig. 13 a). Low values of $\delta^{13}C$ occur in the first interval (0.38‰) and at 15 cm (0.38‰) and high values occur at 10 cm (0.57‰) and 25 cm (0.69‰). A significant increase in $\delta^{13}C$ can be observed between 15-25 cm, here excursions of 0.31‰ were recorded. A fall of 0.2‰ is also observed from 10-15 cm. $\delta^{18}O$ values remains close to the average from 5-20 cm depth and are higher than average in the first interval (4.08‰) and at 25 cm (4.10‰), the latter depth follows a similar increase found in $\delta^{13}C$ but is less significant.

3.2.2. Core HH17-2-971 GC

$\delta^{13}C$ and $\delta^{18}O$ illustrates similar trends excluding 15 cm depth where $\delta^{13}C$ increases and $\delta^{18}O$ decreases (Fig. 13b). The planktonic $\delta^{13}C$ values follow fairly closely to the average core value of 0.56‰ with the exceptions at 5 cm and 40 cm. A low value occurs at 5 cm (0.41‰) creating a trough and a high value is recorded

at 40 cm (0.71‰) where $\delta^{13}C$ peaks. An increase is observed from 25-40 cm of 0.19‰, followed by a fall back to the average. The $\delta^{18}O$ average value is 4.06‰ and shows no major change except the excursion from 30 cm to 60 cm where a fall of 0.16‰ is measured from a high value of 4.16‰.

3.2.3. Core HH17-2-972 GC

$\delta^{13}C$ and $\delta^{18}O$ show similar trends nonetheless $\delta^{13}C$ has exaggerated peaks (Fig. 13c). $\delta^{13}C$ and $\delta^{18}O$ values in the first 15 cm remain close to the average of 0.54‰ and 4.04‰ respectively. A significant increase in $\delta^{13}C$ of 0.22‰ occurs from 25-35 cm forming a peak with the highest value of 0.68‰, values then return back to average. The planktonic $\delta^{18}O$ value at 30 cm was the lowest measured, this is followed by a gradual increase to 4.11‰ at 65 cm.

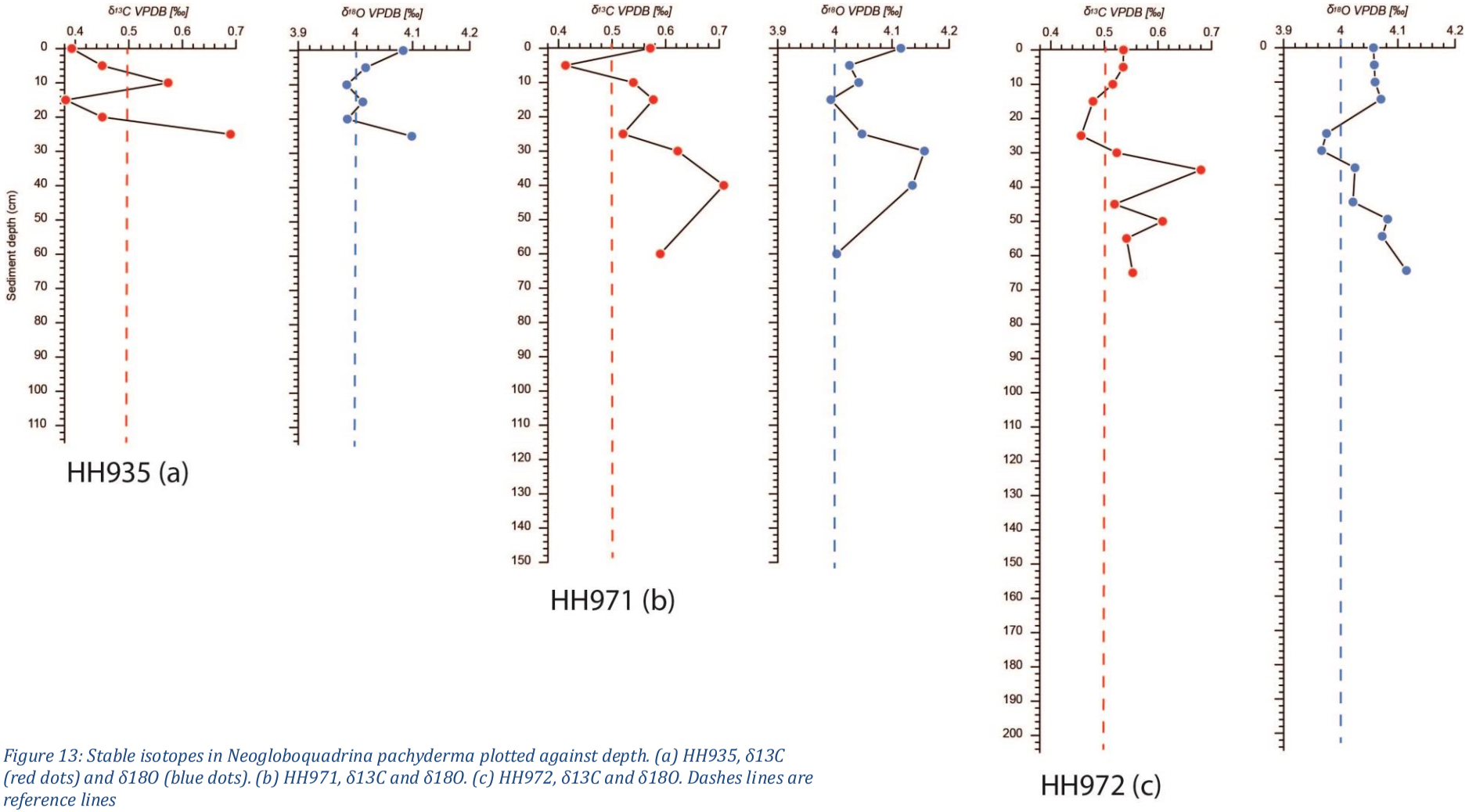

Figure 13: Stable isotopes in Neogloboquadrina pachyderma plotted against depth. (a) HH935, δ13C (red dots) and δ18O (blue dots). (b) HH971, δ13C and δ18O. (c) HH972, δ13C and δ18O. Dashes lines are reference lines

3.3. Organic compounds

Organic compound plots of carbon and nitrogen (Fig. 14) generally show a decreasing trend of $\delta^{13}C$ and $\delta^{15}N$, and C% and N%. Measurements of $\delta^{13}C$ range between -25.9‰ and -23.0‰, and $\delta^{15}N$ range between 2‰ and 7.61‰. Carbon percentages show values between 0.7% - 2.9% and nitrogen percentages between 0.03% - 0.73%. All three cores display a shift where values decrease further and become irregular, this occurs at different depths in each core, 45cm (HH935), 75 cm (HH971), 95 cm (HH972). Roughly at this point $\delta^{13}C$ and $\delta^{15}N$ lines cross over and values fluctuate more than in the upper section. The C% and N% remains fairly parallel throughout the cores with the exception of HH935 where a crossover does occur. HH935 is also the only core where N% values are relatively higher than C% in the upper section.

3.3.1. Core HH17-2-935 GC

$\delta^{13}C$ and $\delta^{15}N$ have an average value of -23.6‰ and 5.7‰ respectively in the upper section where $\delta^{13}C$ is relatively higher than $\delta^{15}N$ (Fig. 14a). This decreases to -25.1‰ and 3.56‰, respectively in the lower section. The upper section values stick closely to the average with little fluctuations. Below 45 cm $\delta^{13}C$ values fluctuates and drops to a low of -25.9‰ at 65 cm where $\delta^{13}C$ is now relatively lower than $\delta^{15}N$, values then increase to follow the average of the lower section. $\delta^{15}N$ values show a gradual decrease to 3.03‰ at 65 cm and continues to follow the $\delta^{15}N$ average core value in the lower section. The C% and N% plot (Fig. 14a) illustrates the same trend except N% is relatively higher than C% in the upper section and is lower in the lower section. C% and N% have an average core value of 1.7% and 0.22% respectively in the upper section and 1.3% and 0.07% in the lower core. Below 45 cm, C% begins to decrease but is followed by a spike to 2.9% at 55 cm. C% values decrease back to the average of the lower section and fluctuates. N%

falls to 1.1% at 50 cm and gradually decreases roughly following the average. C% and N% both show a peak at 90 cm, 1.8% and 0.09% respectively.

3.3.2. Core HH17-2-971 GC

The average core value of $\delta^{13}C$ and $\delta^{15}N$ in the upper section is -23.50‰ and 5.71‰ respectively, and -24.8‰ and 4.01‰ in the lower section (Fig. 14b). Measurements in the first 75 cm follow the average closely. $\delta^{13}C$ seems to be relatively higher than $\delta^{15}N$ but gets closer around 60 cm. The shift here becomes noticeable due to the major fluctuations in data below 75 cm. $\delta^{13}C$ values fall to -25‰ (85 cm), then peaks at 90 cm with -23.6‰. Another drop occurs down to -25.3‰ (100 cm) where values remain close to the average. $\delta^{15}N$ gently decreases below 75 cm with exceptions at 115 cm and 145 cm where peaks of 7.6‰ and 5.8‰ are recorded respectively. C% and N% illustrates a different trend where C% values remain relatively higher than N% throughout the core. N% gently decrease with depth as does C% but with more irregularities. Values stay fairy constant with depth and start to fluctuate slightly below 75 cm. A slight fall in both C% and N% is recorded at 75-80 cm matching the shift in $\delta^{13}C$ and $\delta^{15}N$. The average core value of C% and N% in the upper section is 1.70% and 0.22%, and 1.2% and 0.08% in the lower section.

3.3.3. Core HH17-2-972 GC

$\delta^{15}N$ values remained consistent at 5.69‰ to the depth of 95 cm which was the average for the upper section. $\delta^{13}C$ values also roughly followed the average of -23.5‰ in the upper section while slightly decreasing. $\delta^{13}C$ and $\delta^{15}N$ values both fell at 95 cm (Fig. 14c). $\delta^{15}N$ fell to 3.63‰ close to the lower section average of 3.16‰ and remained consistent with depth. $\delta^{13}C$ fell to -25.4‰ and fluctuated also close to the average of -25‰ at 100 cm and hit a low of -25.9‰ at 125 cm remaining consistent with slight variations. The C% and N% trend is very similar to

the one illustrated in HH971 (Fig. 14b) with upper section averages of 1.8% (C%) and 0.2% (N%) and lower section average of 1.5% (C%) and 0.07% (N%). N% values gently decrease with depth while C% remain consistent in the upper section and fluctuate slightly in the lower section.

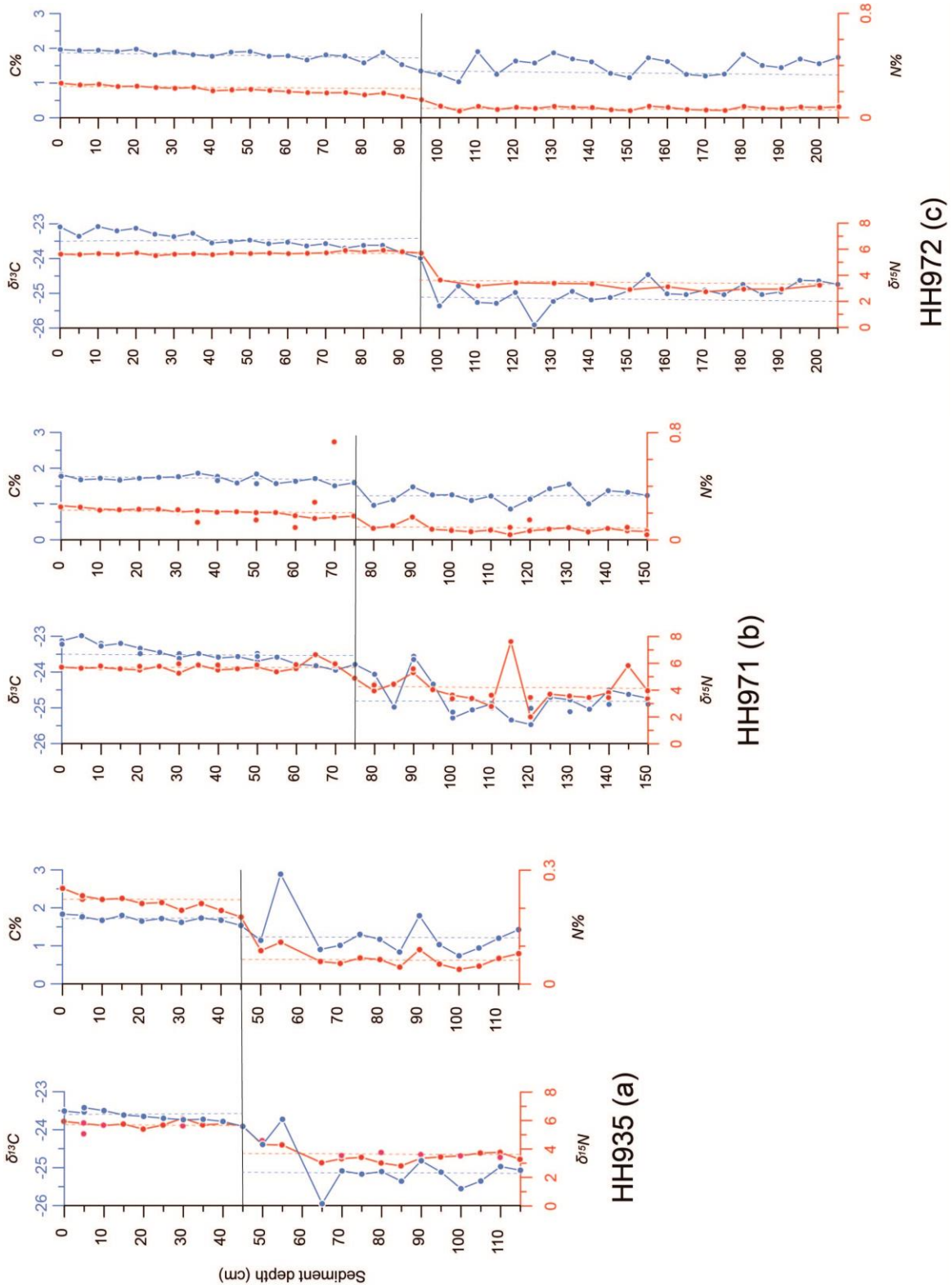

Figure 14: Organic compound plots for HH935 (a), HH971 (b), HH972 (c). δ13C, δ15N, C% and N% values are plotted against depth. Horizontal black line separates the upper and lower section in each core. Red and blue dashed lines illustrate core average. Blue dots indicate carbon values and red dots indicate

3.4. X-ray fluorescence (XRF)

3.4.1. HH17-2-935 GC

The Fe/Ca ratio shows a dramatic drop at approximately 70 cm bsf which is not seen in any other core. This drop is shown in the XFR imagery as a band of brown sediment and separates the olive grey laminated sediment in the top from the dark grey laminated sediment in the bottom. The upper section of the core displays high values in Fe/Ca and Br/Cl and lower values in the bottom section of the core which matches the trend in the other two cores (Fig. 15a). Zr/Rb values have the opposite trend with low values in the upper section and high values in the lower section which also matching the trend in the other two cores. The transition from high to low values or vice versa occurs at roughly the same depth as the fall in Fe/Ca.

3.4.2. HH17-2-971 GC

Elemental ratios in Figure 15b all illustrate a shift at approximately 85 cm bsf and is shown in the XRF imagery by a change in sediment colour from olive grey to dark grey. Fe/Ca ratio follows a similar trend to HH935 but instead of a fall, Fe increases sharply then drops very slow making way for high Ca values in the lower core. The Zr/Rb ratio shows a clear trend with low values in the upper section and high values in the lower section. The Br/Cl ratio also shows a similar trend to Fe/Ca but with a gradual decrease at 80 cm bsf.

3.4.3. HH17-2-972 GC

All three ratios in Figure 15c show the same trend as the other two cores but with the shift occurring at 105 cm bsf also shown in the XRF imagery by a change in colour. Fe/Ca does not show any major change at the transition point, just a smooth decline correlating with the increase in Zr/Rb.

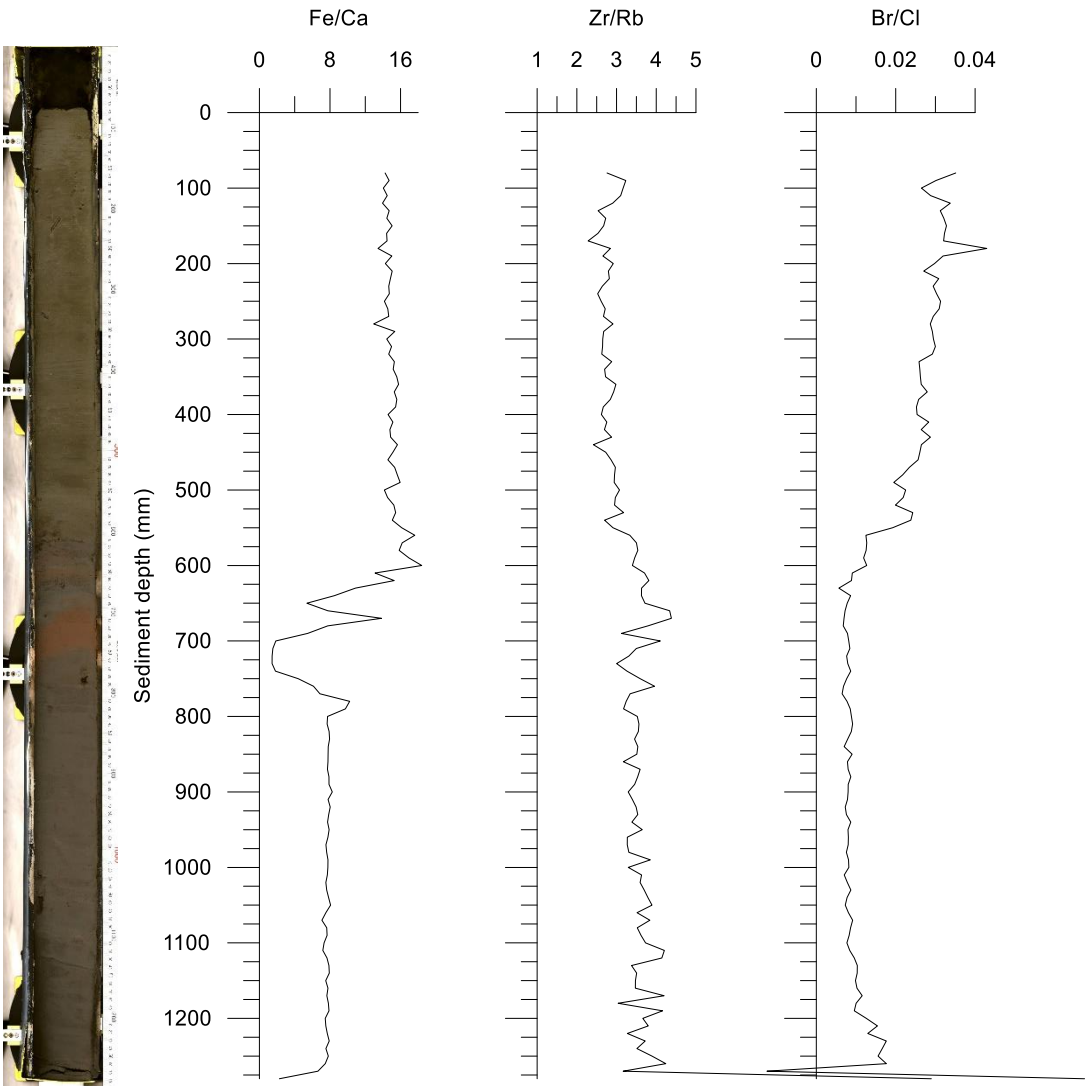

(a) HH935

Figure 15 (a): XRF elemental ratios of Fe/Ca, Zr/Rb and Br/Cl for core HH935 and XRF imagery along the y-axis

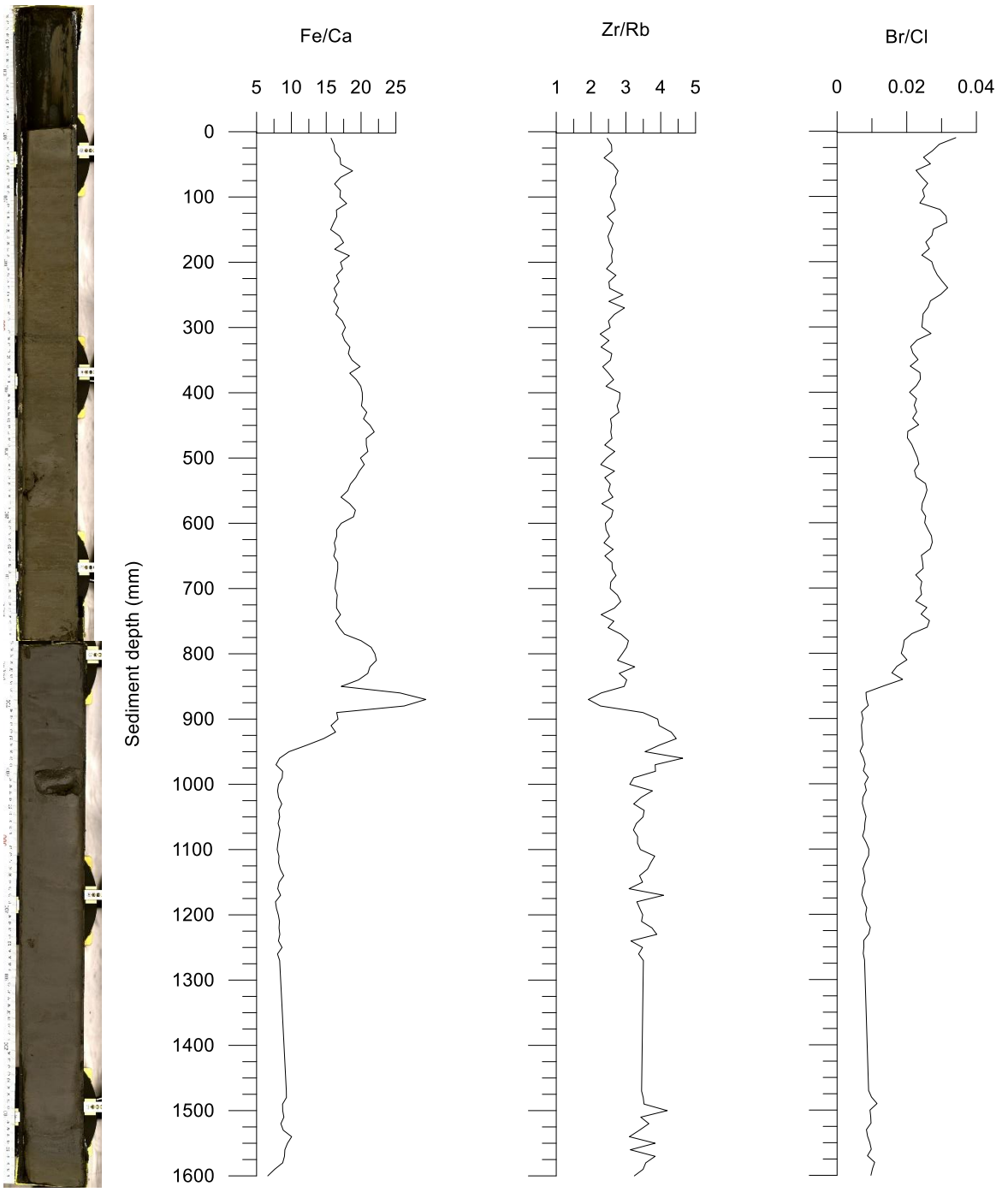

(b) HH971

Figure 15 (b): XRF elemental ratios of Fe/Ca, Zr/Rb and Br/Cl for core HH971 and XRF imagery along the y-axis

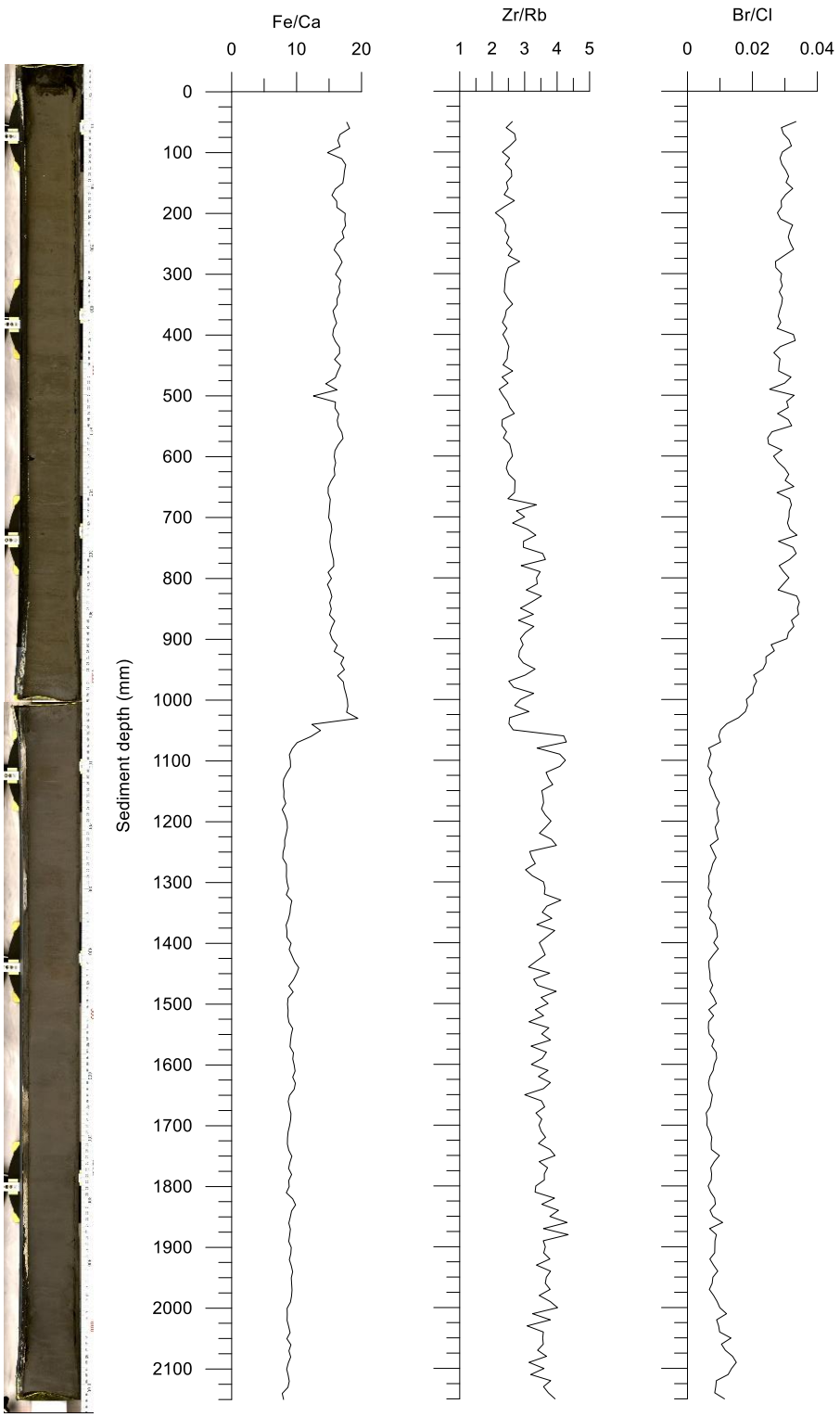

(c) HH972

Figure 15 (c): XRF elemental ratios of Fe/Ca, Zr/Rb and Br/Cl for core HH972 and XRF imagery along the y-axis

4. Discussion and interpretation

The descriptions and interpretations of the identified units in this study begins with the oldest unit that is present in all the cores.

4.1. Foraminifera association

The following foraminifera descriptions are of major species that were recorded from cores HH935, HH971 and HH972. These species will be used as an environmental proxy in this investigation.

Melonis barleeanus (Williamson, 1858) is a common species amongst deep sea Quaternary benthic foraminifera. Increasing abundance of *M. barleeanus* has been associated with cooling trends by Lutze, (1977) and Loubere and Banonis, (1987) noticed a correlation between interglacial conditions and *M. barleeanus* abundance. This species has been known to tolerate low oxygen content in organic rich sediment (Fontanier *et al.*, 2002) and is associated with degraded organic matter (Wollenburg, Knies and Mackensen, 2004; Dijkstra *et al.*, 2015). High percentages have also been linked to constant bottom currents indicated by Murray (1984).

Cibicidoides lobatulus (Walker & Jacob, 1878) is a sessile foraminifera with an epifaunal lifestyle. It lives in current influenced environments and is very likely to be transported after death (Boltovskoy & Wright, 1976). *Cibicidoides lobatulus* is most commonly confined to sea bottom areas in the Barents Sea that are exposed to currents (Korsun *etal.,* 1990) and also thrives in river distal areas (Polyak *et al.*, 2002).

Elphidium excavatum (Terquem, 1875) is known to thrive in stressed environments where temperatures and salinity levels are low along with short productivity periods (Hald *et al.,1*993). They are widespread on Arctic shelves and are typically in high abundance near glacier environment. This species is also found frequently

in late Quaternary glaciomarine sediments in the north (Hald and Vorren, 1987). Studies by Hald *et al.* (1993) illustrated that *E. excavatum* is common in Arctic Bottom Water and in sea ice covered areas.

Astrononion gallowayi (Loeblich & Tappan, 1953) is an epifaunal species that prefers distal-river and shallow areas. High abundance can be related to currents flowing on shallow shelf areas and is indicative of high energy environments (Polyak *et al.*, 2002; Jennings *et al.*, 2004). *This species* prefers temperatures < 1°C and high salinity (Steinsund *et al.*, 1994).

Cassidulina reniforme (Nørvang, 1945) is an infaunal Arctic benthic species typically found in glaciomarine environments and cold waters, for example the Norwegian Sea Bottom Water (Hald and Korsun, 1997) and prefers seasonal sea-ice cover, low salinity and temperatures < 2°C (Polyak *et al.*, 2002).

Cassidulina neoteretis (Seidenkrantz, 1995) can be a shallow infaunal dweller or an epifaunal species (Steinsund *et al.* 1994). *Cassidulina neoteretis* is commonly found in fjord and shelf environments with normal salinity and favours cold bottom waters by following cold Atlantic waters and muddy sea floors (Hald and Korsun, 1997).

Buccella frigida (Cushman, 1922) has been linked to high seasonal productivity and sea ice cover in the Arctic (Lubowska *et al.*, 2005). According to Steinsund *et al.* (1994), *B. frigida* prefers temperatures between 0-1°C and a salinity of 33-34‰. Their plano-convex test shape indicates their epifaunal nature.

Islandiella norcrossi (Cushman, 1933) has a relatively high seasonal productivity in low Arctic environments where there is seasonal ice sheets (Mudie *et al.*, 1984). Data from Polyak *et al.* (2002) indicate high abundances occur where there is seasonal sea ice, which can be associated with summer ice-edge productivity.

In the following section *E. excavatum, A. gallowayi, C. lobatulus, C. neoteretis* and *I. norcrossi* will be used to understand and reconstruct the paleoenvironment of the cores due to their clear links to Atlantic water flow and ice cover.

Biological productivity was absent in the lower section of all three cores. This was due to permanent ice sheet cover throughout Unit 2 which began to retreat during the transition period towards the end of the unit resulting in very little or no planktic and benthic foraminifera being preserved. Descriptions of the units are found in the paleoenvironment reconstruction section.

The diversity and specific richness of benthic foraminiferal assemblages directly reflects the quality and availability of food, substrate, oxygen, salinity and bottom water temperatures (Wollenburg *et al*., 1998). A study conducted by Wollenburg and Kuhnt (2001) established that benthic foraminiferal species in the Arctic Ocean and western Svalbard are drawn to fresh organic material. Organic compounds data shown in Figure 15 illustrates high total organic carbon (TOC) and total nitrogen in Unit 1 which implies quality organic matter, this decreases in Units 2 which results in poor organic matter reflecting the decrease in foraminiferal densities. The foraminiferal fauna in Unit 1 is significantly diverse and rich. HH935 is the only core to have very few foraminifera present in Unit 2 (Fig. 15). This can be linked to the appearance of brown oxidized sediment shown in the XRF imagery (Fig. 15) at approximately 70 cm bsf, which indicates a well ventilated bottom environment (Ivanova *et al.*, 2002). Species found at this depth include insignificant amounts of *A. gallowayi, C. reniforme and B. frigida,* and significant numbers of *E. excavatum* and *C. lobatulus* (Table 5). *Cibicidoides lobatulus* is indicative of high energy environments suggesting that the periodical nepheloid flow that formed the brown sediment developed from winter brines during sea ice freezing (Ivanova *et al.*, 2002) and flowed during this time forming an oxic environment for foraminifera production. Wollenburg and Mackensen, (1998) proposed that if *C. lobatulus* detached from the substrate it could live infaunally. The presence of *E.*

excavatum at this depth correlates with *C. lobatulus* as environmental indicators. *Elphidium excavatum* is common on Arctic shelves and can be found in high abundance in areas with fluctuating environments (Hald and Korsun, 1997). Hald and Steinsund, (1994) presented that *E. excavatum* is related to Arctic Bottom Water and sea ice. *Astrononion gallowayi* shows an increasing trend towards the top of the core and *E. excavatum* shows a decreasing trend towards the top of the core (Fig. 15). *Elphidium excavatum* is linked to areas with fluctuating environments and sea ice cover. The increasing percentage of this species with depth follow this assumption as *E. excavatum* abundance increases closer to the unit boundary where the environment transitions from to seasonal sea ice to permanent sea ice. *Astrononion gallowayi* shows high abundances in the top of Unit 1 suggesting that the area is under the influence of strong currents. *Cassidulina neoteretis* is very abundant only in HH971. Abundance is low in the first 30 cm bsf then spikes to 11.6% followed by a drop and other spike at 75 cm bsf with an abundance of 17.9%. This species is distributed between water depths of 200 and 1400 m and is thus used as an indicator for Atlantic water in benthic foraminiferal studies (Wollenburg *et al.,* 2004). The decrease in *C. neoteretis* is linked to cold Atlantic Waters (Dijkstra *et al.*, 2015) which reflects the high abundance of *A. gallowayi*. We can therefore assume that during these periods of low abundance, cold Atlantic water influenced the environment and warm Atlantic waters influenced times of high abundance, for example at 40 cm bsf. This reflects with the fall in abundance of *E. excavatum* at the same depth which prefers colder temperatures and ice cover (Fig 15). *Islandiella norcrossi* abundances have been liked to seasonal ice-free environments by Polyak and Solheim, (1994). Figure 15 illustrates roughly that high abundances in *I. norcrossi* relates to the low abundances of *E. excavatum*. This relation can point out times of high seasonal ice and ice-free conditions. For example, HH971 shows an increase in *E. excavatum* abundance at 30 cm bsf while *I. norcrossi* decreases dramatically, suggesting a seasonal ice cover (Fig. 15).

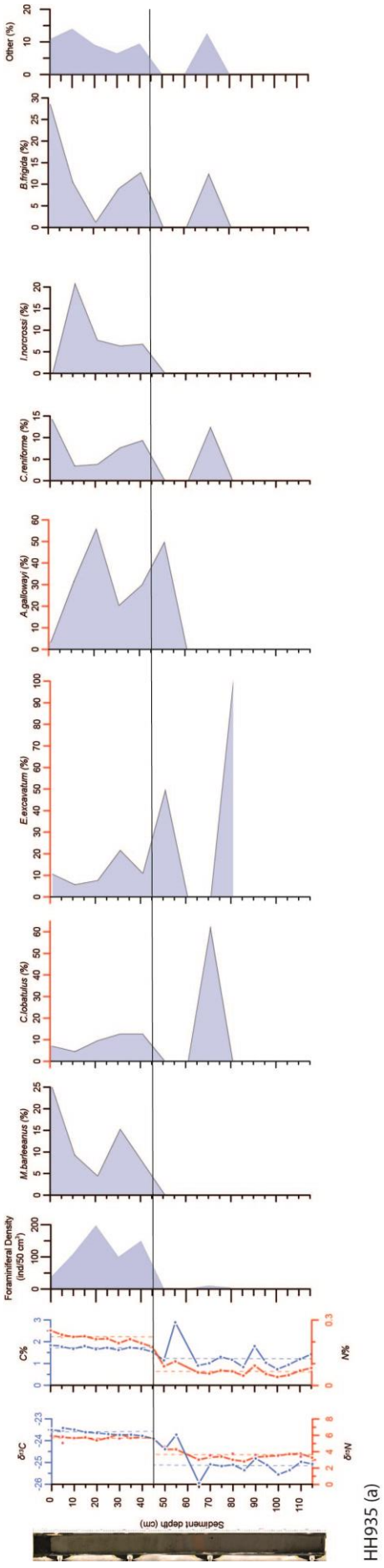

Figure 15 (a): Foraminiferal abundance of major species correlated with XRF imagery and organic compounds.

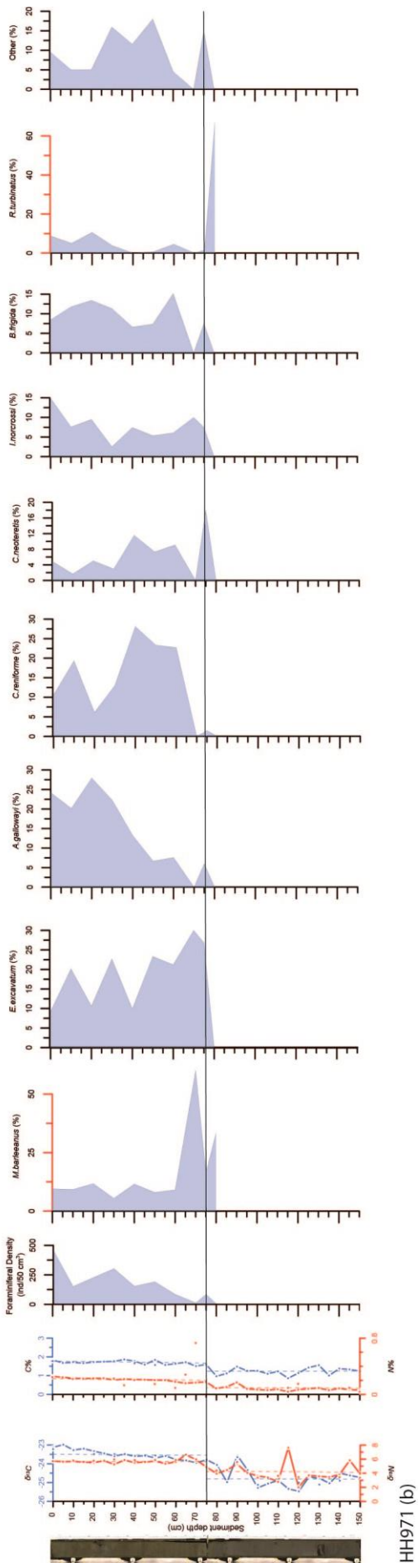

Figure 25 (b): Foraminiferal abundance of major species correlated with XRF imagery and organic compounds.

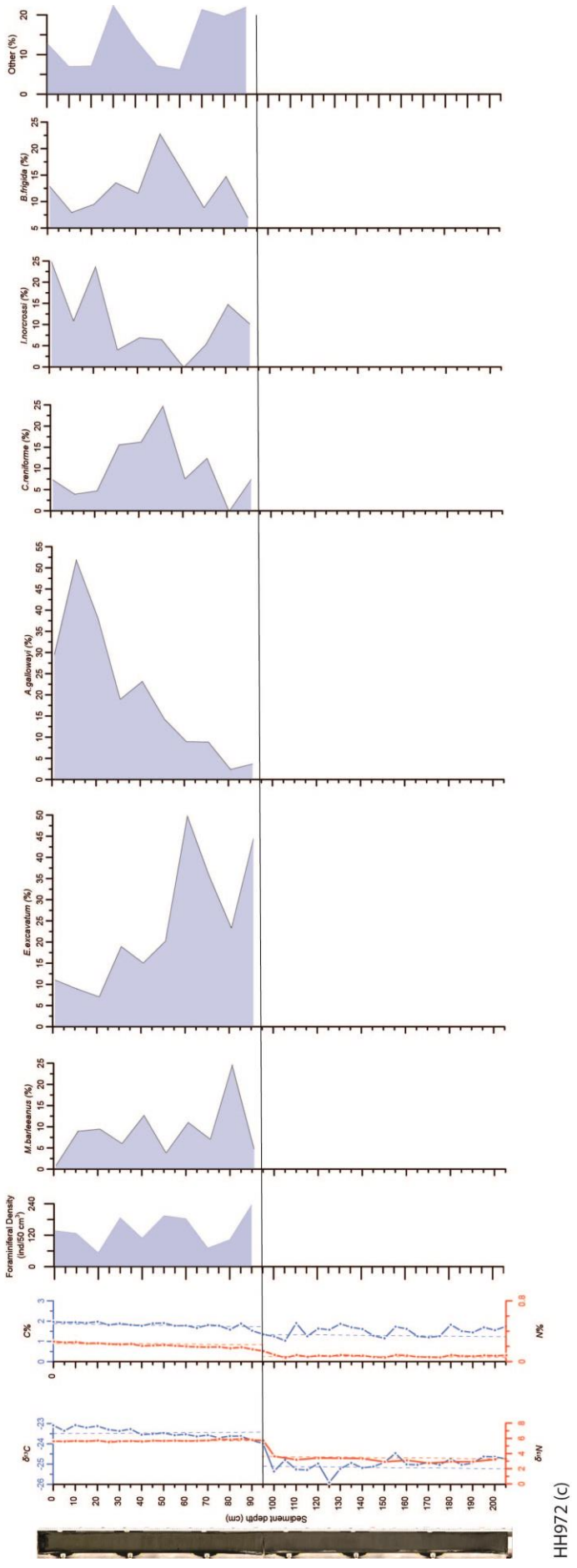

Figure 35 (c): Foraminiferal abundance of major species correlated with XRF imagery and organic compounds.

4.2. Paleoenvironment reconstruction

Many studies have been carried out referring to the shift from the Late Weichselian into the Holocene in the Barents Sea. The dramatic environmental changes that took place during this time have been related to deglaciation, climatic warming, glacio-eustatic sea level rise and warm Atlantic waters (Lubinski *et al.*, 1996; Duplessy *et al.*, 2001). The three gravity cores illustrated in Figure 19 exhibit two units dividing the Late Weichselian from the Holocene. These units were also identified by comparing the data sets collected to similar studies undertaken by Lucchi *et al.* (2013), Ivanova *et al.* (2002), Duplessy *et al.* (2005), and Rüther *et al.* (2017). Ivanova *et al.* (2002) and Duplessy *et al.* (2005) collected sediment cores from several Barents Sea shelf depressions one of which in proximity to HH936, HH971 and HH972 study area. The table below shows the details of the 3 cores extracted by Ivanova and Duplessy.

Station No.	Latitude (N)	Longitude (E)	Water depth (m)	Recovery (m)	Thickness of stratigraphic units (m)		
					I	II	III
ASV 880	79°55.5′	47°08.2′	388	5.08	3.10	0.94	0.90
ASV 1183	71°28.3′	40°48.3′	330	4.17	2.63	1.54	–
ASV 1200	75°54.4′	41°00.5′	308	3.60	2.25	0.47	1.88

Table 7: Sediment core locations, depth and thickness from (Ivanova et al., 2002)

Core ASV 1200 was extracted from the Persey Trough close to the centre of the Barents Sea, south east of R/V Helmer Hansen gravity core locations. This comparison was chosen not only due to location similarities but also because, both locations are under the influence of the Polar Front. Rüther's investigation site is found in the uppermost section of Bjørnøyrenna, North-West of the Olga Basin. 5 gravity cores were extracted on shallow areas where there were signs of MSGL and crevasse squeeze ridges. Core 354 was collected slightly deeper than the rest and is similar to this investigation as there is no sign of grounded ice. A deglaciation age is also established which will be looked into in the following

section. Lucchi *et al.* (2013) investigated the mechanism of sediment transport on the Storfjorden and Kveithola trough-mouth fans (TMF) during deglaciation and used the Ca/Ti ratio to aid in dividing the stratigraphic units. This ratio illustrates the calcium concentrations against the titanium detrital phase. Chirp sub-bottom profiles across depressions one and two from the CAGE 17-2 research cruise measured sediments up to 15 m thick in D1, surrounding areas between depressions had limited cover indicating that depressions acted as a sediment trap. Each identified unit is indicative of a particular paleoenvironment and depending on how the ice sheets moved during this time, boundaries may be diachronous (Ivanova *et al.*, 2002). Since this is not a detailed sedimentological investigation the term 'unit' is used to divide stratigraphy. A unit is defined as a volume of sediment with a relative age range and a particular set of characteristics such as colour and grain size. There was some hesitation when dividing the units, it is clear that the base of Unit 1 resides at 95 cm bsf in HH972 due to abrupt changes in water content, Ca/Ti ratio, and organic compounds, as well as sediment colour. In the lower section of the core there was a possibility to divide it into two units forming a transition unit just under Unit 1 which would be defined by the brown oxidized layer at 65 cm bsf in HH935 and a fall in the Ca/Ti ratio in HH971 and HH972. This idea was seen unnecessary due to lack of lithological evidence and the fact that the brown layer only occurs in HH935. Therefore, Unit 2 defines the entire bottom section of the cores.

4.2.1. Unit 2

Unit 2 is found in the bottom section of all 3 cores (HH935, HH971 and HH972) and corresponds to similar units from other cores in the Barents Sea (Fig. 16) (Ivanova *et al.*, 2002; Duplessy *et al.*, 2005). The laminated sediment here consists of dark grey, fine grained sediment deposited by sea ice melt suggesting cyclic sedimentation and is barren in foraminifera. Samples showed consistent

appearance of minor ice-rafted debris (IRD) with the exception of a large rounded stone lodged in gravity core HH971 at 140 cm depth. Along with this information and sedimentological descriptions by Rüther *et al.* (2017) we can define the sediment in Unit 2 as a matrix supported glacial till. The lack of foraminifera and presence of IRD led to the assumption that

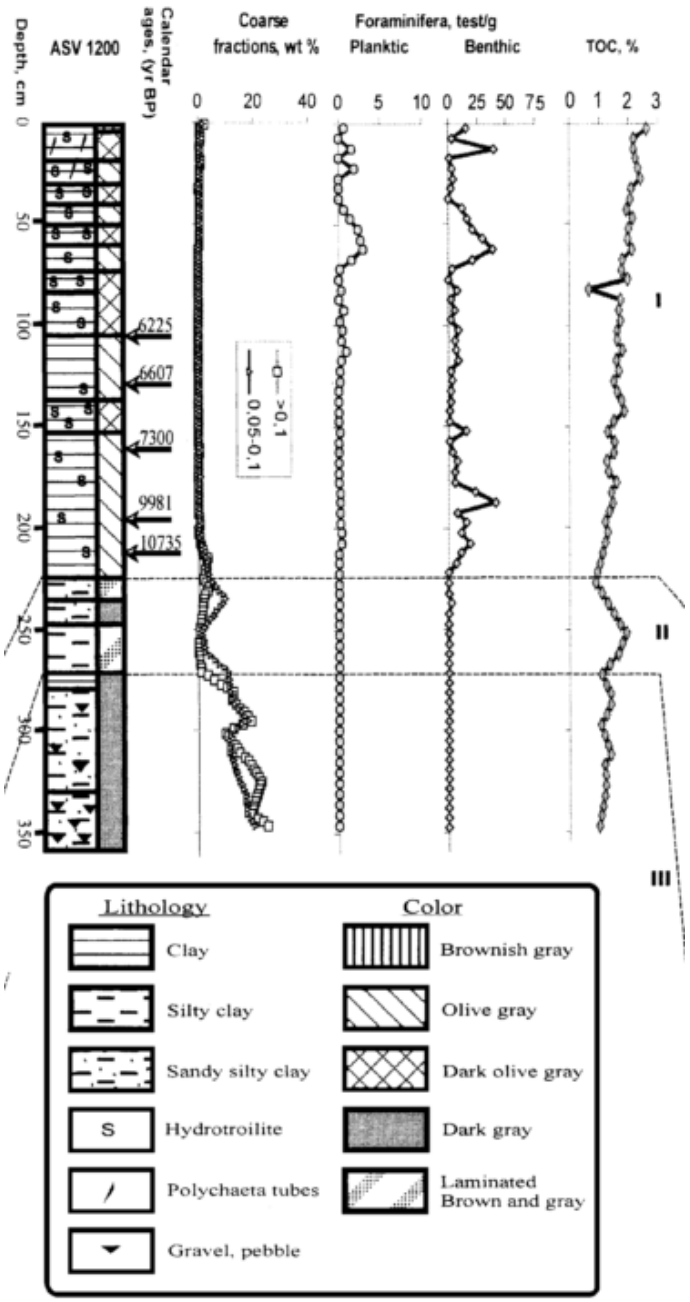

Figure 16: Unit division of core ASV 1200 by Ivanova et al. 2002.

Unit 2 was deposited in permanent sea ice setting which resulted in settling of fine grained sediment and slowed down biological activity. Pyrite minerals are scattered through this section along with some green minerals olivine and black glassy minerals. Pyrite formation controls the oxygen level and sulphate concentration in seawater and results from the reaction of hydrogen sulphide (H_2S) from bacterial sulphate reduction with iron minerals. The amount of pyrite that forms is controlled by the supply rate of decomposable organic matter, dissolved sulphate and reactive lithic fragments of iron minerals (Berner, 1984). This explains the decrease in organic matter shown by the organic compounds and Br/Cl ratio (Fig 17). Other XRF results show high calcium values in Unit 2 even with no biological production because the iron, shown in the Fe/Ca ratio is being used in the formation of pyrite (Fig. 17). Unit 2 is already a low oxygen environment due to ice cover which promoted the growth of pyrite.

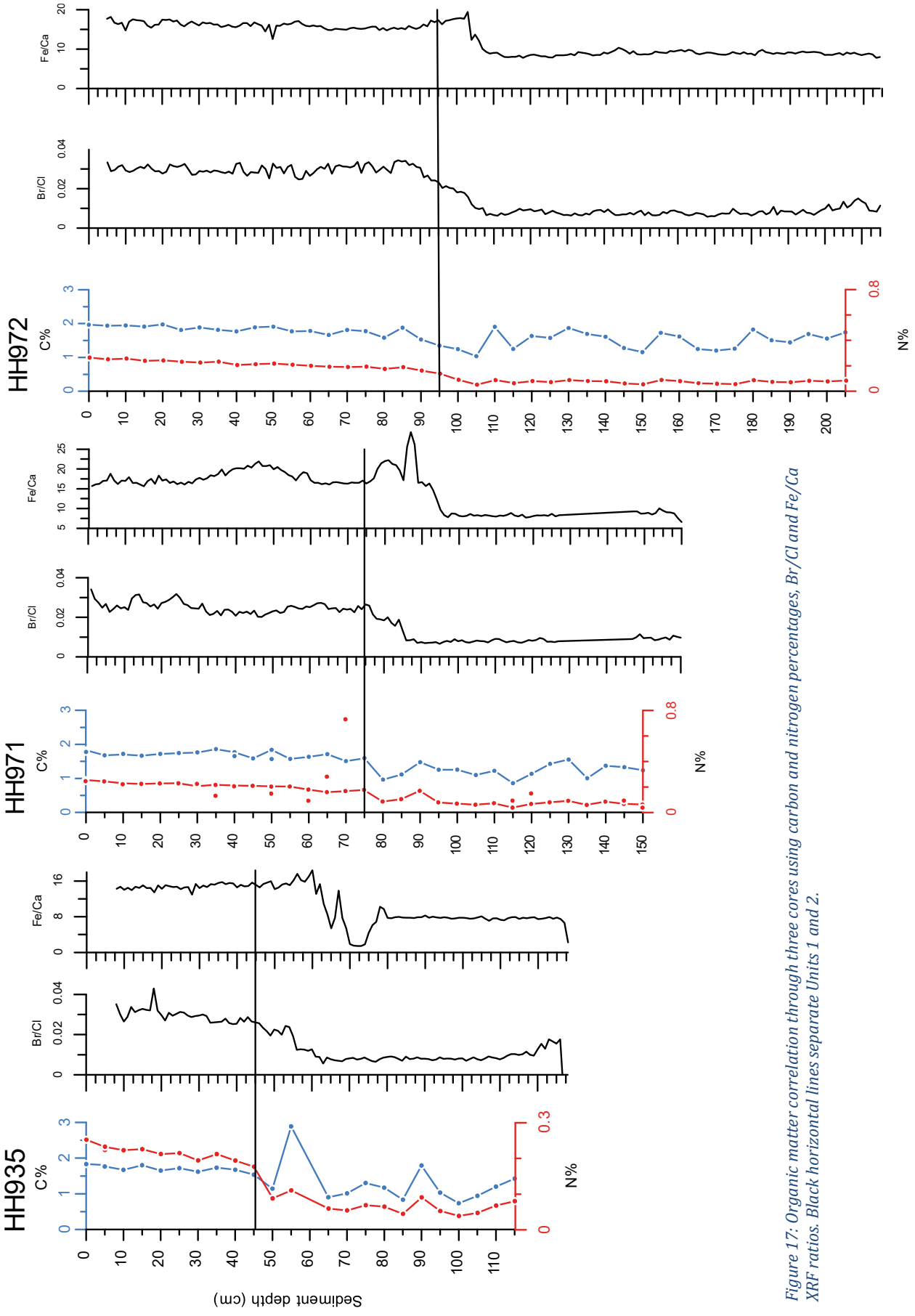

Figure 17: Organic matter correlation through three cores using carbon and nitrogen percentages, Br/Cl and Fe/Ca XRF ratios. Black horizontal lines separate Units 1 and 2.

The water content in this unit is low (17-19%) in all three cores which would normally suggest that the sediment has been subjected to compression by a glacial load, if this occurred no sedimentation should take place, in-fact the opposite would occur as grounded ice would cause erosion of the sea floor. By looking at the Zr/Rb XRF ratio which is a common indicator for grain size (Taylor, 1965), it can be observed that the larger grain size related to sea ice cover in this unit reflects the water content as larger grains retain less water. Towards the boundary between Unit 1 and 2 water content increases dramatically this is observed in the Zr/Rb ratio as material becomes finer marking a transitional phase (Fig. 22).

Due to climatic warming and sea level rise, the first phase of ice sheet retreat from the Barents Sea shelves is recorded approximately 13 ka BP (Lubinski *et al.*, 1996; Polyak and Mikhailov, 1996)**.** Ice sheet retreat from Bjørnøyrenna to Storbankenrenna is explain in further detail in the next section. This ice retreat marked the transition from permanent sea ice environment to seasonal sea ice environment. This shift in environment is shown by an increase in water content of all three gravity cores and fall in the Ca/Ti ratio for HH971 and HH972 but a positive spike in HH935 (Fig. 19). During this transition phase Ca/Ti decreases and increases in HH971 and HH972. HH935 is located approximately 6 km from the depressions D1 in D2 to the west which is where the Ca/Ti ratio spikes radically at 65 cm bsf. By referring to the XRF imagery of HH935 we can correlate this spike to the brown sedimentation that occurs towards the top of Unit 2 (Fig 18). This brown oxidized layer is only found in HH935. According to Ivanova *et al.* (2002), this brown and grey laminated sequence in the transition phase suggests rapid build-up of cyclic sediment from a nepheloid flow with slow, irregular sedimentation into a sediment trap in a ventilated bottom setting. This oxygenated setting resulted in higher calcium content in the sediment and which is not found in any other core, hence this nepheloid flow occurs presumably only in this area.

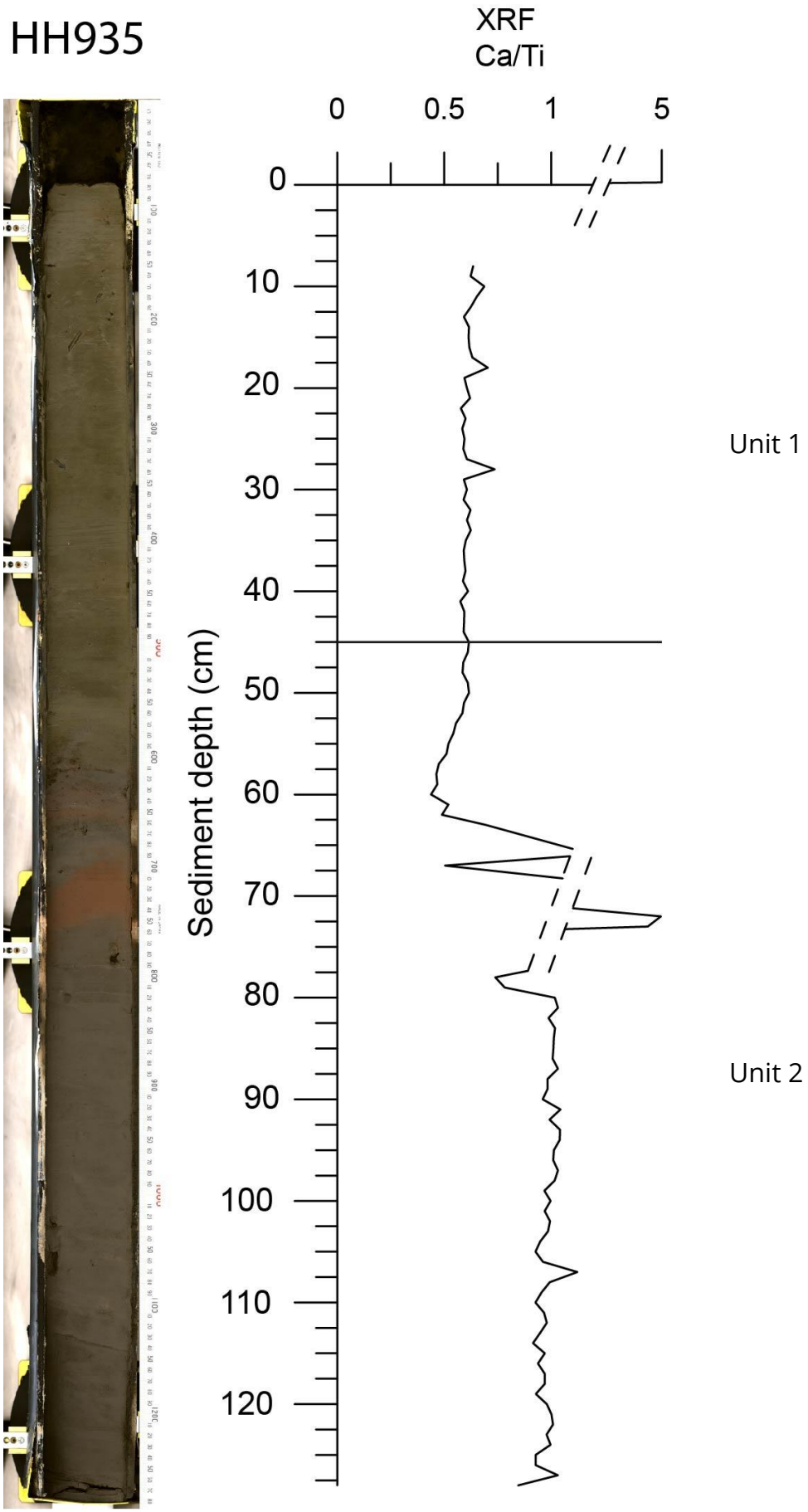

Figure 18: Oxidized sediments in HH935 linked to high calcium in the transition phase of Unit 2

4.2.2. Unit 1

Unit 1 is characterized by fine grained olive-grey laminated clay and a variety of foraminifera, benthic macrofauna and bryozoans which marks the change from the transitioning period of permanent sea ice to marine conditions with seasonal sea ice. Total organic carbon (TOC) is fairly high in this unit (1.5-2%) along with increasing total Nitrogen (0.16-0.26%) indicating increased quality of organic matter (Fig. 17).

The planktonic species *Neogloboquadrina pachyderma* is found frequently in the top section of the unit but is scarce towards the bottom and benthic foraminifera abundance is generally high. This increase in biological productivity at the unit boundary is possible linked to seasonal ice-free conditions related to warming and the Atlantic water inflow, into the Barents Sea.

A sharp boundary is observed in the XRF imagery between Units 1 and 2 in HH971, HH935 shows a gradual change which included the brown layer previously mentioned and HH972 also shoes a gradual change. During this environmental shift the colour of sediment deviates from the dark grey in Unit 2 to olive grey. This sharp boundary indicates a dramatic alteration in the palaeoceanographic conditions of the Barents Sea. According to AMS dating of sample 95-96 cm, HH972, this change occurred approximately 9.7 ka BP. Sediment supply and transport variations, along with paleoproductivity associated with migration of the Polar Front and sea ice margin which rests on the intensity of Atlantic water flowing into the Barents Sea, controlled the development of Holocene environments.

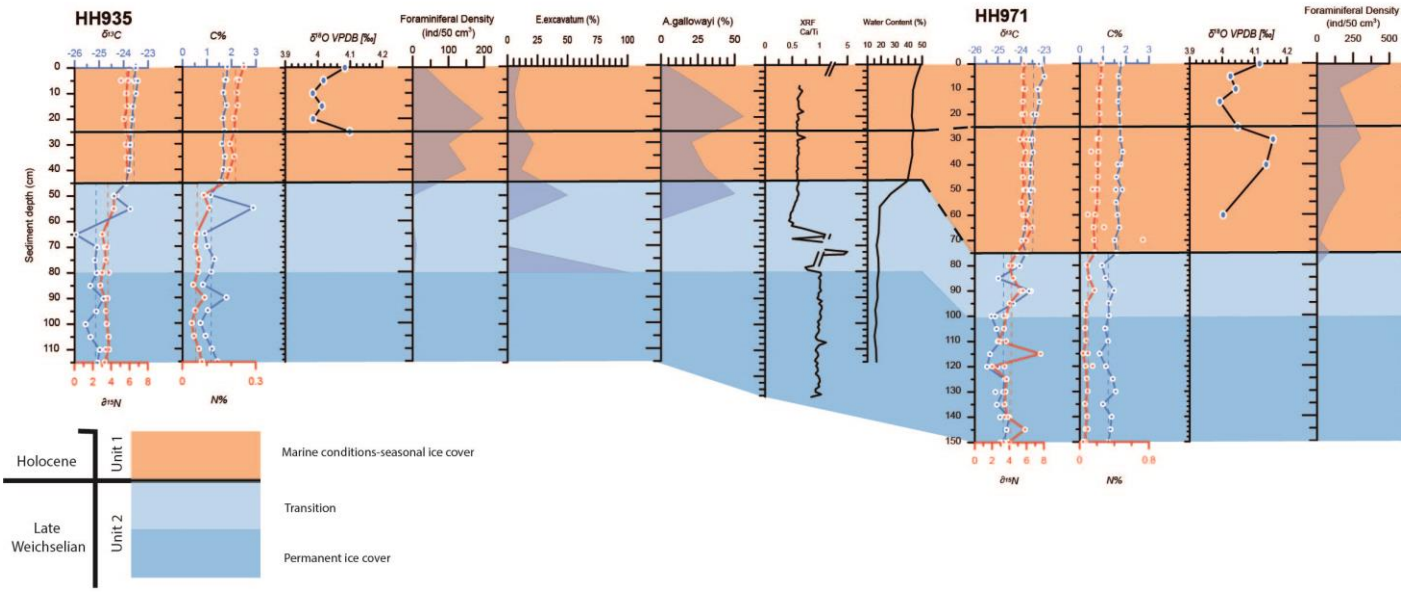
HH935
HH971
Sediment depth (cm)
Foraminiferal Density (ind/50 cm³)
E.excavatum (%)
A.gallowayi (%)
XRF Ca/Ti
Water Content (%)
C%
N%
Holocene
Late Weichselian
Unit 1
Unit 2
Marine conditions-seasonal ice cover
Transition
Permanent ice cover

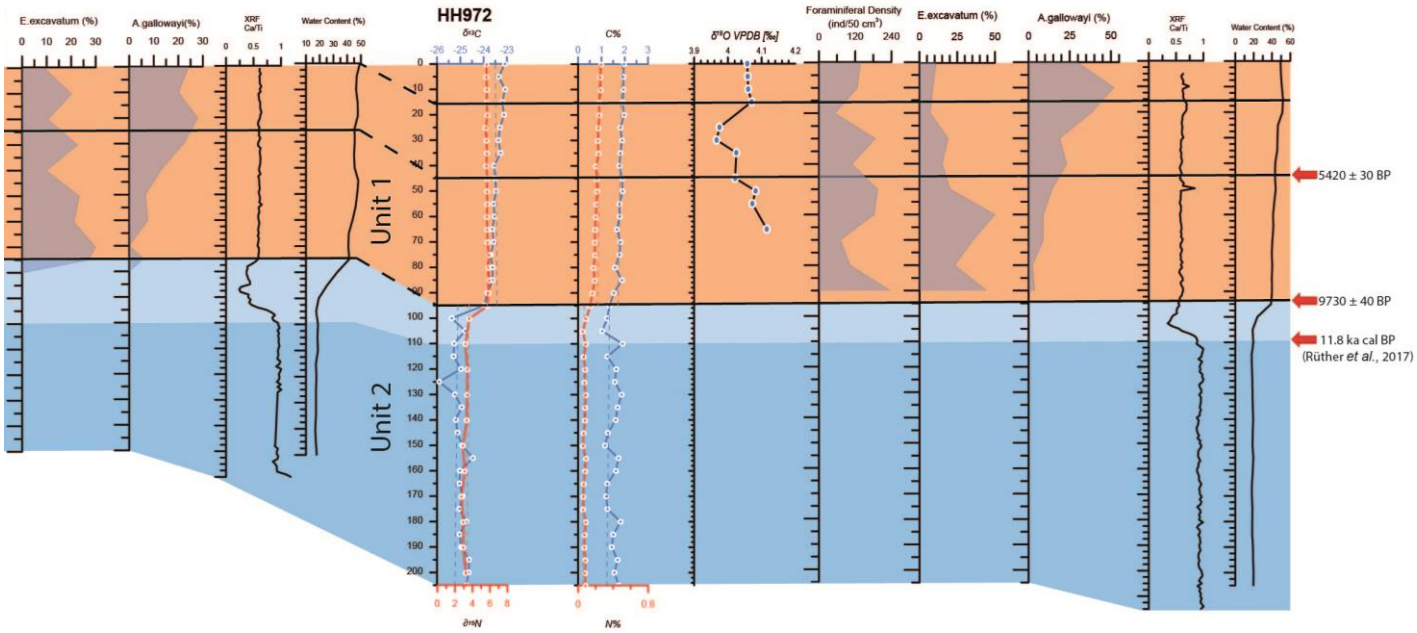

Figure 19: HH935, HH971 and HH972 correlation. Different coloured sections indicate changing environments and red arrows show AMS radiocarbon dating ages.

4.3. Ice Sheets

AMS radiocarbon dating results at 95-96 cm in core HH972 confirms the age of the base of Unit 1 at 9730 ± 40 BP, slightly younger than the age at which the Holocene began approximately 11,650 years before present (Walker *et al.*, 2009)(Fig. 19). It is therefore possible to infer that the non-glaciogenic sediments in Unit 1 are Holocene in age and Unit 2 consists of glaciomarine deposits linked to the Late Weichselian Glaciation.

4.3.1. Late Weichselian Glaciation

During this time the entire Barents Sea continental shelf was glaciated by the Barents Sea Ice Sheet (BSIS). Details of the approximate timing of deglaciation are unclear. Vorren and Laberg, (1996) and Landvik *et al.* (1998) stated that deglaciation on the western margin started 17.5 cal ka BP which resulted in most of the Barents Sea being ice free by approximately 15 cal ka BP. The first stage of retreat in the Bjørnøyrenna occurred around 16.9–17.5 cal ka BP and according to Rüther *et al.* (2017), the BSIS was completely fragmented during the beginning of the Holocene, which was shown by elevated beaches on Kong Karls Land with dates of 11.1–11.6 ka cal BP. Ice retreat along the western margin of the Barents Sea has been studied extensively (e.g., Elverhøi *et al.,* 1982; Nielsen and Rasmussen, 2017) but little is known about the retreat patterns in the central Barents Sea where the gravity cores in this study were collected. The ice flow through Storbanken across Storbankrenna was slower than in Bjørnøyrenna due to less meltwater. New geological data presented in Bjarnadóttir *et al.* (2014) is used in the attempt to understand the dynamics of the ice sheets in this area. Two main flow directions were identified using ice flow indicators such as Mega Scale Glacial Lineation's (MSGL). The first of which flows in a NW-SE direction in Storbankrennas western flank and ENE-WSW in the other parts of the trough (Fig. 23). Bjarnadóttir et al. (2014) inferred that

the ice retreated slowly through Bjørnøyrenna and up to Storbanken across Storbankrenna which is approximately where the gravity cores were extracted (Fig. 23). Figure 20 (Patton *et al.*, 2015) shows the general ice cover and flow directions of deglaciation in the Barents Sea during the Late Weichselian glaciation.

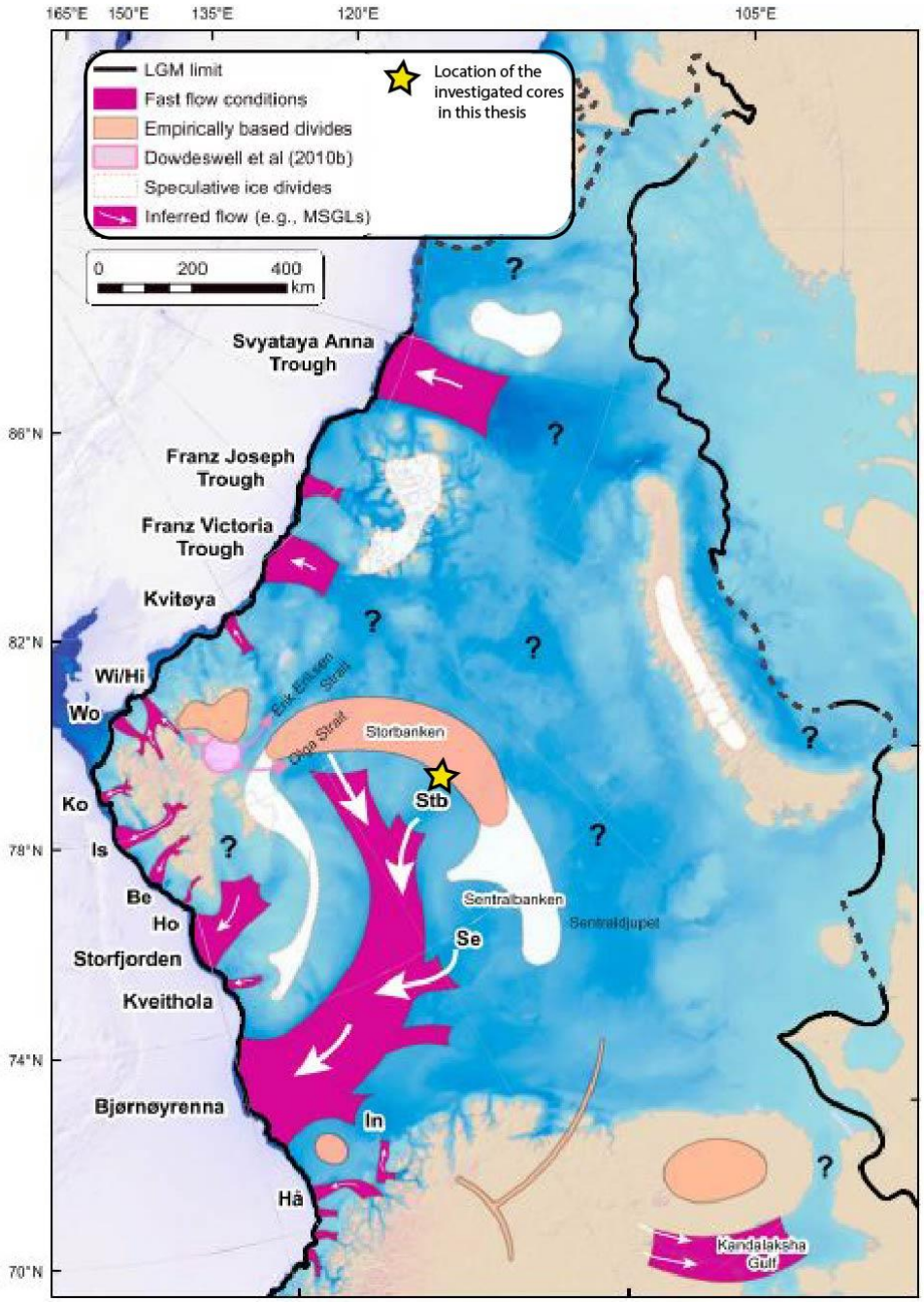

Figure 20: BSIS LGM extent and deglaciation pathways (Patton et al., 2015). Be = Bellsund, Hi = Hinlopen Trough, Ho = Hornsund, Hå = Håkjerringdjupet, In = Ingøydjupet, Is=Isfjorden, Ko=Kongsfjorden, Se=Sentralbankrenna, Stb=Storbankrenna,Wi=Wijdefjorden Trough, and Wo=Woodfjorden Trough

The lack of foraminifera observed in Unit 2 from the foraminiferal study strengthens the idea of permanent sea ice cover during this period as ice cover inhibits biological productivity by restricting oxygen flow and organic matter to the sea floor. The age of BSIS fragmentation proposed by Rüther *et al.* (2017) roughly coincides with the transitional environment between permanent ice and seasonal ice. A deglaciation age of approximately 11.8 ka cal BP is measured in core 354 by Rüther *et al.* (2017) (Fig. 21). Even though the units defined in this study does not match our investigation it is possible to use this information and assume that the transition phase towards the end of Unit 2 began 11.8 ka cal BP marking the deglaciation in our study area.

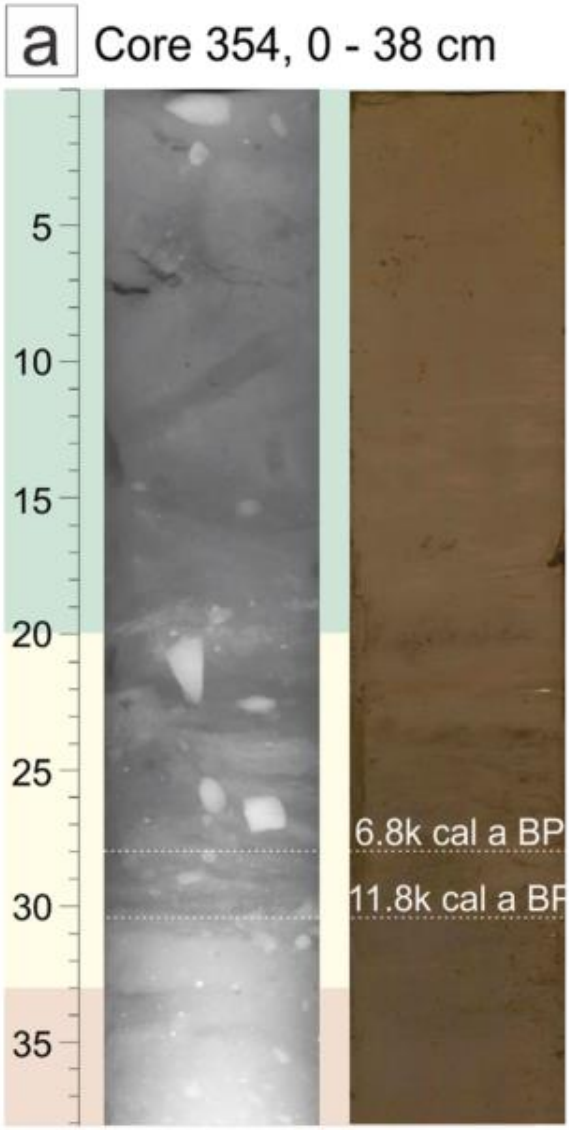

Figure 41: Radiographs and photographs of core 354 from Rüther et al. (2017) showing deglaciation age

The XRF ratio Zr/Rb (Fig. 22) can be used to determine ice cover. Zr/Rb values are high in Unit 2 in all three cores indicating a courser grain than in Unit 1. This reflects the low water content and results from the settling of fine grained sediment from melt water due to permanent ice cover which also deposited minor IRD.

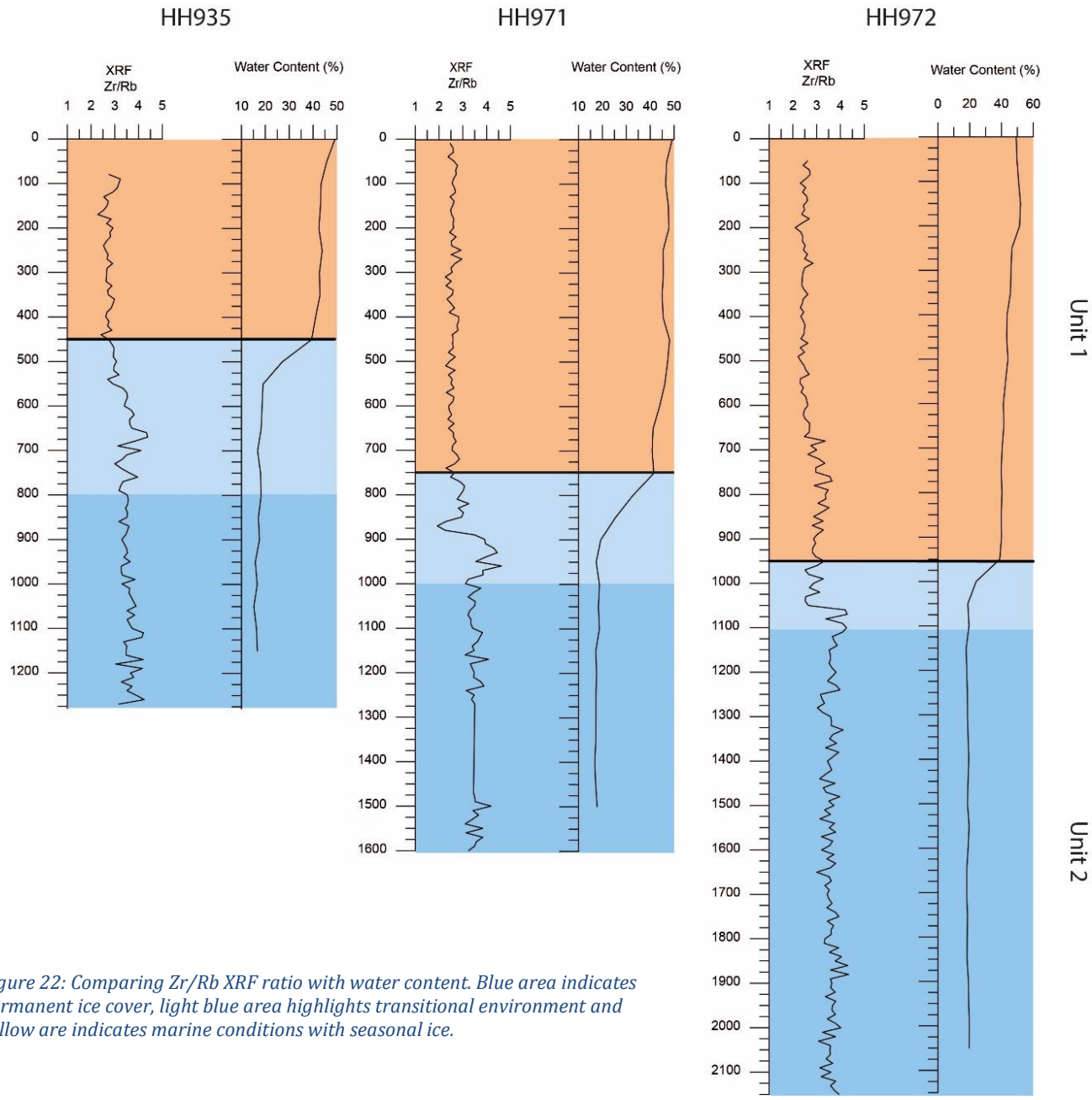

Figure 22: Comparing Zr/Rb XRF ratio with water content. Blue area indicates permanent ice cover, light blue area highlights transitional environment and yellow are indicates marine conditions with seasonal ice.

4.3.2. Holocene

During this transitional period the Barents Sea ice disintegrated and retreated through Storbankrenna to an ice dome predicted by Lambeck, (1995) on Storbanken. Figure 23 (from Bjarnadóttir *et al*., 2014) shows detailed ice retreat through Storbankrenna during the inferred transition phase. The olive grey sediments of Unit 1 are rich in organic debris and foraminifera suggesting high biological productivity related to seasonally ice-free conditions. Foraminifera such as *E. excavatum* and *C. reniforme* that are present also prefer seasonal ice. Zr/Rb ratio shows that very finer material is located in Unit 1 which directly relates to the high-water content and seasonal ice as terrigenous material is being deposited from the continents into the basin during the Holocene (Fig. 22).

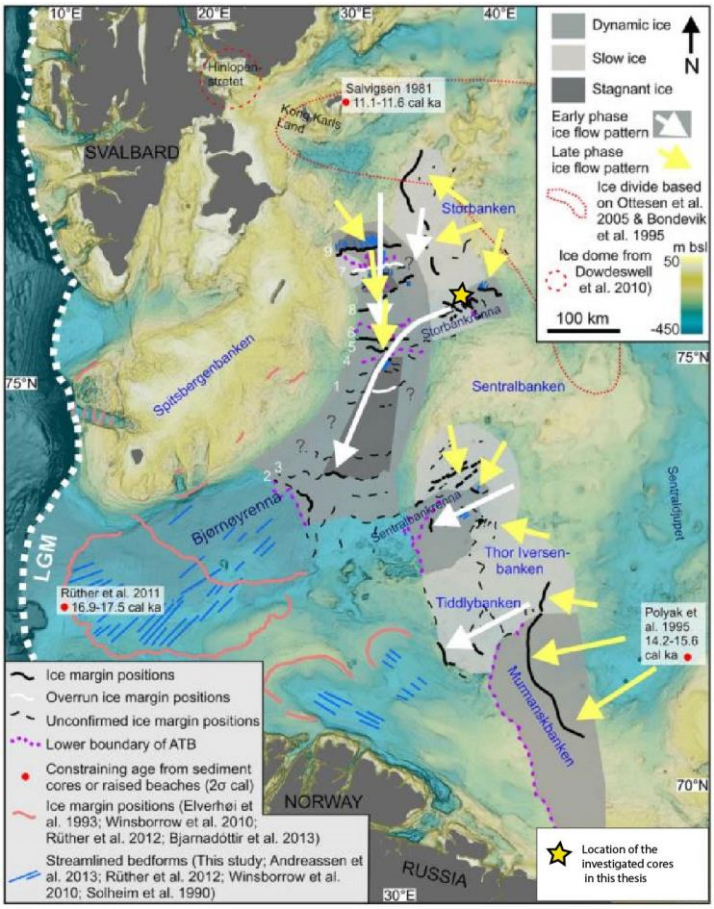

Figure 23: Reconstruction of ice retreat in the Barents Sea showing main paleo ice flow orientations. Shaded areas illustrate speed of flow indicated in the key. Taken from (Bjarnadóttir et al. 2014)

5. Summary and conclusion

Three gravity cores were collected from the Olga Basin in the central Barents Sea which underwent foraminiferal investigation, stable isotope, organic compounds and element geochemistry analysis. This led to two distinct units being identified and the reconstruction of paleoenvironment and ice sheet transition.

AMS radiocarbon dating along with relevant literature established Unit 1 as Holocene in age and Unit 2 as Late Weichselian.

Unit 2 defines the lower section of the cores and is characterized by a glacial till which is barren in foraminifera, has a dark grey colour and low water and organic matter content. Due to very low foraminiferal abundance of this unit and fine-grained sediment with the presence of IRD, permanent ice cover is expected. The low organic matter content was linked to the low oxygen environment due to the sea ice which prompted the formation of pyrite in the sediments.

Towards the end of Unit 2 a transition phase is established from decreasing values of the Ca/Ti ratio. By referring to Rüther *et al.* (2017), an age of 11.8 ka cal BP was determined to mark the beginning of this transition. During this time, HH935 recorded an oxygen input which stemmed from Arctic bottom waters forming nepheloid flows, indicating that D2 was under the influence of polar waters.

Unit 1 in the upper section of the core is characterized by high foraminiferal density, olive grey colour and high organic matter and water content. The environment shifts from low energy at the bottom of the unit to high energy at the top. The foraminiferal data collected cannot determine the exact periods of Arctic and Atlantic water influence due to some contradicting interpretations, nevertheless, we can assume the Arctic front winnowing through this area and seasonal ice cover due to the reflecting relationship between *I. norcrossi* and *E. excavatum*.

References

Aagaard, K., Foldvik, A. and Hillman, S. R. (1987) 'The West Spitsbergen Current: Disposition and water mass transformation', Journal of Geophysical Research. Wiley-Blackwell, 92(C4), p. 3778. doi: 10.1029/JC092iC04p03778.

Adegbie, A. T. et al. (2003) 'Glacial millennial-scale fluctuations in central African precipitation recorded in terrigenous sediment supply and freshwater signals offshore Cameroon', Palaeogeography, Palaeoclimatology, Palaeoecology. Elsevier, 197(3–4), pp. 323–333. doi: 10.1016/S0031-0182(03)00474-7.

Antonsen, P., Elverhoi, A., Dypvik, H. and Solheim, A. (1991) 'NW-Barents-Olga-Basin-Shallow-Bedrock-Geology-'. AAPG, p. pp.1178-1194.

Auriac, A. et al. (2016) 'Glacial isostatic adjustment associated with the Barents Sea ice sheet: A modelling inter-comparison', Quaternary Science Reviews. Pergamon, 147, pp. 122–135. doi: 10.1016/J.QUASCIREV.2016.02.011.

Bauch, D., Carstens, J. and Wefer, G. (1997) 'Oxygen isotope composition of living Neogloboquadrina pachyderma (sin.) in the Arctic Ocean', Earth and Planetary Science Letters. Elsevier, 146(1–2), pp. 47–58. doi: 10.1016/S0012-821X(96)00211-7.

Beta Analytic Inc. (1990) 'Introduction to Radiocarbon Determination by the Accelerator Mass Spectrometry Method', (1), pp. 1–16. Available at: http://www.radiocarbon.com/accelerator-mass-spectrometry.htm.

Bjarnadóttir, L. R., Winsborrow, M. C. M. and Andreassen, K. (2014) 'Deglaciation of the central Barents Sea', Quaternary Science Reviews. Pergamon, 92, pp. 208–226. doi: 10.1016/J.QUASCIREV.2013.09.012.

Boltovskoy, E. & Wright, R. 1976. Recent Foraminifera. Dr W. Junk, The Hague

Bosak, T. et al. (2011) ‘Agglutinated tests in post-Sturtian cap carbonates of Namibia and Mongolia’, Earth and Planetary Science Letters. Elsevier, 308(1–2), pp. 29–40. doi: 10.1016/J.EPSL.2011.05.030.

Calvert, S. E. and Pedersen, T. F. (2007) ‘Chapter Fourteen Elemental Proxies for Palaeoclimatic and Palaeoceanographic Variability in Marine Sediments: Interpretation and Application’, Developments in Marine Geology. Elsevier, 1, pp. 567–644. doi: 10.1016/S1572-5480(07)01019-6.

Carstens, Jö. and Wefer, G. (1992) ‘Recent distribution of planktonic foraminifera in the Nansen Basin, Arctic Ocean’, Deep Sea Research Part A, Oceanographic Research Papers, 39(2 PART 1). doi: 10.1016/S0198-0149(06)80018-X.

Dijkstra, N. et al. (2015) ‘Natural variability of benthic foraminiferal assemblages and metal concentrations during the last 150years in the Ingøydjupet trough, SW Barents Sea’, Marine Micropaleontology. Elsevier B.V., 121, pp. 16–31. doi: 10.1016/j.marmicro.2015.09.005.

Dowdeswell, J. A. et al. (1996) ‘Large-scale sedimentation on the glacier-influenced polar North Atlantic Margins: Long-range side-scan sonar evidence’, Geophysical Research Letters. Wiley-Blackwell, 23(24), pp. 3535–3538. doi: 10.1029/96GL03484.

Duplessy, J. C. et al. (2005) ‘Paleoceanography of the Barents Sea during the Holocene’, Paleoceanography. Wiley-Blackwell, 20(4), p. n/a-n/a. doi: 10.1029/2004PA001116.

Duplessy, J. et al. (2001) ‘Holocene paleoceanography of the northern Barents Sea and variations of the northward heat transport by the Atlantic Ocean’, Boreas, 30, pp. 2–16. Available at: https://onlinelibrary.wiley.com/doi/pdf/10.1111/j.1502-3885.2001.tb00984.x

Elverhøi, A., Solheim, A. and Eluerhgi andAnders Solheim, A. (1982) 'The Barents Sea ice sheet -a sedimentological discussion'. Available at: https://www.tandfonline.com/doi/pdf/10.3402/polar.v1i1.6968?needAccess=true

Esteves, M. et al. (2017) 'Retreat patterns and dynamics of the Sentralbankrenna glacial system, central Barents Sea', Quaternary Science Reviews. Pergamon, 169, pp. 131–147. doi: 10.1016/J.QUASCIREV.2017.06.004.

Fisher, T. (no date) 'Thermo Scientific GasBench II: The Universal On-Line Gas Preparation and Introduction System for Isotope RatioMS', in.

Fontanier, C. et al. (2002) 'Live benthic foraminiferal faunas from the Bay of Biscay: faunal density, composition, and microhabitats', Deep-Sea Research I, 49, pp. 751–785. Available at: http://epic.awi.de/4960/1/Fon2002a.pdf (Accessed: 5 June 2018).

Freudenthal, T. et al. (2001) 'Early diagenesis of organic matter from sediments of the eastern subtropical Atlantic: evidence from stable nitrogen and carbon isotopes', Geochimica et Cosmochimica Acta. Pergamon, 65(11), pp. 1795–1808. doi: 10.1016/S0016-7037(01)00554-3.

Hald, M. and Korsun, S. (1997) 'Distribution of modern benthic foraminifera from fjords of Svalbard, European Arctic', The Journal of Foraminiferal Research, 27(2), pp. 101–122. doi: 10.2113/gsjfr.27.2.101.

Hald, M. and Vorren, T. O. (1987) 'Foraminiferal stratigraphy and environment of Late Weichselian deposits on the continental shelf off Troms, northern Norway', Marine Micropaleontology. Elsevier, 12, pp. 129–160. doi: 10.1016/0377-8398(87)90018-1.

Ivanova, E. V et al. (2002) ‘Late Weichselian to Holocene paleoenvironments in the Barents Sea’, Global and Planetary Change. Elsevier, 34(3–4), pp. 209–218. doi: 10.1016/S0921-8181(02)00116-9.

Ivanova, E. V et al. (2002) ‘Late Weichselian to Holocene paleoenvironments in the Barents Sea’, Global and Planetary Change. Elsevier, 34(3–4), pp. 209–218. doi: 10.1016/S0921-8181(02)00116-9.

Jennings, A. E. et al. (2004) ‘Modern Foraminiferal Faunas of the Southwestern to Northern Iceland Shelf: Oceanographic and Environmental Controls’, Journal of Foraminiferal Research, 34(3), pp. 180–207. Available at: https://gsw.silverchair-cdn.com/gsw/Content_public/Journal/jfr/34/3/10.2113_34.3.180/2/fora-34-302-180.pdf?Expires=1527260398&Signature=gRYDh7oJmVMmvke2suwFHx6kO6FdHZZZ5NQ17JmKIDcbbssYvUXzCZr0kzemkuOKHaOk9mw-C-8N1ZaBXS98qtgU6mSHlZaZksrWVI3THb9zupwxlKgUS0K (Accessed: 24 May 2018).

Lambeck, K. (1995) ‘Constraints on the Late Weichselian ice sheet over the Barents Sea from observations of raised shorelines’, Quaternary Science Reviews. Pergamon, 14(1), pp. 1–16. doi: 10.1016/0277-3791(94)00107-M.

Lambeck, K. (1995) ‘Constraints on the Late Weichselian ice sheet over the Barents Sea from observations of raised shorelines’, Quaternary Science Reviews. Pergamon, 14(1), pp. 1–16. doi: 10.1016/0277-3791(94)00107-M.

Landvik, J. Y. et al. (1998) ‘The last glacial maximum of Svalbard and the Barents Sea area: Ice sheet extent and configuration’, Quaternary Science Reviews, 17(1–3), pp. 43–75. doi: 10.1016/S0277-3791(97)00066-8.

Loeng, H. (1991) ‘Features of the physical oceanographic conditions of the Barents Sea’, Polar Research, 10(1), pp. 12–16. Available at:

https://www.tandfonline.com/doi/pdf/10.3402/polar.v10i1.6723 (Accessed: 30 April 2018).

Loubere, P. and Banonis, G. (1987) 'Benthic foraminiferal assemblage response to the onset of northern hemisphere glaciation: Paleoenvironmental changes and species trends in the northeast Atlantic', Marine Micropaleontology. Elsevier, 12, pp. 161–181. doi: 10.1016/0377-8398(87)90019-3.

Lubinski, D. J. Et al. (1996) 'The last deglaciation of the Franz Victoria Trough, northern Barents Sea', Boreas. Wiley/Blackwell (10.1111), 25(2), pp. 89–100. doi: 10.1111/j.1502-3885.1996.tb00838.x.

Lubowska, M. A. et al. (2005) 'Changes in the flow of Atlantic water into the Arctic Ocean since the last deglaciation: Evidence from the northern Svalbard continental margin, 80°N'. doi: 10.1029/2005PA001141.

Lucchi, R. G. et al. (2013) 'Postglacial sedimentary processes on the Storfjorden and Kveithola trough mouth fans: Significance of extreme glacimarine sedimentation', Global and Planetary Change. Elsevier B.V., 111, pp. 309–326. doi: 10.1016/j.gloplacha.2013.10.008.

Lutze, G. F. (1977) '1. Benthic Foraminifers at Site 397: Faunal Fluctuations and Ranges in The Quaternary Introduction And Methods'. Available at: http://deepseadrilling.org/47_1/volume/dsdp47pt1_11.pdf (Accessed: 24 May 2018).

Mamo, B. L., Brock, G. A. and Gretton, E. J. (2013) 'Deep sea benthic foraminifera as proxies for palaeoclimatic fluctuations in the New Caledonia Basin, over the last 140,000 years', Marine Micropaleontology. Elsevier, 104, pp. 1–13. doi: 10.1016/J.MARMICRO.2013.08.002.

Midttun, L. (1985) 'Formation of dense bottom water in the Barents Sea', Deep

Sea Research Part A. Oceanographic Research Papers. Elsevier, 32(10), pp. 1233–1241. doi: 10.1016/0198-0149(85)90006-8.

Mudie, P. J. et al. (1984) 'Multivariate analysis and quantitative paleoecology of benthic foraminifera in surface and Late Quaternary shelf sediments, northern Canada', Marine Micropaleontology. Elsevier, 8(4), pp. 283–313. doi: 10.1016/0377-8398(84)90018-5.

Murray, J. W. and Weston, J. F. (1984) '9. Paleogene and Neogene Benthic Foraminifers from Rockall Plateau 1 With a contribution'. Available at: http://www.deepseadrilling.org/81/volume/dsdp81_09.pdf (Accessed: 24 May 2018).

Murray, J.W., 2006. Ecology and Applications of Benthic Foraminifera. Cambridge University Press.

Nielsen, T. and Rasmussen, T. L. (2017) 'Reconstruction of ice sheet retreat after the Last Glacial maximum in Storfjorden, southern Svalbard', Marine Geology. Elsevier. doi: 10.1016/J.MARGEO.2017.12.003.

Nikolitsa Alexandropoulou, Bruvik Kine, Vincent Carrier, Dessandier Pierre-Antoine, Knut Ola Dølven, Valberg Espen, Dan Fornari, Friederike Gründger, Gregory J. Kurras, Yao Haoyi, Truls Holm, Lindgren Matteus, Katarzyna Melaniuk, Bjorn Runar Olsen, Siri, M. F. S. (2017) Cruise report CAGE 17-2 AMGG.

Ogrinc, N. et al. (2005) 'Carbon and nitrogen isotope compositions of organic matter in coastal marine sediments (the Gulf of Trieste, N Adriatic Sea): indicators of sources and preservation', Marine Chemistry. Elsevier, 95(3–4), pp. 163–181. doi: 10.1016/J.MARCHEM.2004.09.003.

Owens, N.J.P., 1985. Variations in the natural abundance of 15N in estuarine suspended particulate matter: a specific indicator of biological processing.

Estuar. Coast. Shelf Sci. 20, 505–510

Patton, H. et al. (2015) ‘Geophysical constraints on the dynamics and retreat of the Barents Sea ice sheet as a paleobenchmark for models of marine ice sheet deglaciation’, Reviews of Geophysics. Wiley-Blackwell, 53(4), pp. 1051–1098. doi: 10.1002/2015RG000495.

Polyak, L. and Solheim, A. (1994) ‘Late-and postglacial environments in the northern Barents Sea west of Franz Josef Land’, Polar Research. Wiley/Blackwell (10.1111), 13(2), pp. 197–207. doi: 10.1111/j.1751-8369.1994.tb00449.x.

Polyak, L. et al. (2002) ‘Benthic Foraminiferal Assemblages from the Southern Kara Sea, A River-Influenced Arctic Marine Environment’, The Journal of Foraminiferal Research. GeoScienceWorld, 32(3), pp. 252–273. doi: 10.2113/32.3.252.

Rasmussen, T. L. et al. (2007) ‘Paleoceanographic evolution of the SW Svalbard margin (76°N) since 20,000 14C yr BP’, Quaternary Research. Cambridge University Press, 67(1), pp. 100–114. doi: 10.1016/j.yqres.2006.07.002.

Rothwell, R. G. and Croudace, I. W. (2015) Micro-XRF Studies of Sediment Cores. doi: 10.1007/978-94-017-9849-5.

Rothwell, R. G. and Rack, F. R. (2006) ‘New techniques in sediment core analysis: an introduction’, Geological Society, London, Special Publications. Geological Society of London, 267(1), pp. 1–29. doi: 10.1144/GSL.SP.2006.267.01.01.

Rüther, D. C. et al. (2017) ‘Grounding line proximal sediment characteristics at a marine-based, late-stage ice stream margin’, Journal of Quaternary Science. Wiley-Blackwell, 32(4), pp. 463–474. doi: 10.1002/jqs.2939.

Schneider, R. R. et al. (1997) ‘Monsoon related variations in Zaire (Congo)

sediment load and influence of fluvial silicate supply on marine productivity in the east equatorial Atlantic during the last 200,000 years', Paleoceanography. Wiley-Blackwell, 12(3), pp. 463–481. doi: 10.1029/96PA03640.

Standard, T. G. and Ms, I. R. (no date) 'The Gold Standard for Isotope Ratio MS'.

Steinsund, P. I. and Hald, M. (1994) 'Recent calcium carbonate dissolution in the Barents Sea: Paleoceanographic applications', Marine Geology. Elsevier, 117(1–4), pp. 303–316.

Steinsund, P. I. and Hald, M. (1994) 'Recent calcium carbonate dissolution in the Barents Sea: Paleoceanographic applications', Marine Geology. Elsevier, 117(1–4), pp. 303–316.

Stuut, J.-B. W., Temmesfeld, F. and De Deckker, P. (2014) 'A 550 ka record of aeolian activity near North West Cape, Australia: inferences from grain-size distributions and bulk chemistry of SE Indian Ocean deep-sea sediments', Quaternary Science Reviews. Pergamon, 83, pp. 83–94. doi: 10.1016/J.QUASCIREV.2013.11.003.

Svendsen, J. I. et al. (2004) 'Late Quaternary ice sheet history of northern Eurasia', Quaternary Science Reviews. Pergamon, 23(11–13), pp. 1229–1271. doi: 10.1016/J.QUASCIREV.2003.12.008.

Sztybor, K. and Rasmussen, T. L. (2017) 'Late glacial and deglacial palaeoceanographic changes at Vestnesa Ridge, Fram Strait: Methane seep versus non-seep environments', Palaeogeography, Palaeoclimatology, Palaeoecology. Elsevier, 476, pp. 77–89. doi: 10.1016/J.PALAEO.2017.04.001.

Taylor, S. R. (1965) 'The application of trace element data to problems in petrology', Physics and Chemistry of the Earth, 6(C), pp. 133–213. doi: 10.1016/0079-1946(65)90014-5.

Tesdal, J.-E., Galbraith, E. D. and Kienast, M. (2013) 'Nitrogen isotopes in bulk marine sediment: linking seafloor observations with subseafloor records', Biogeosciences, 10, pp. 101–118. doi: 10.5194/bg-10-101-2013.

Thomson, J., Croudace, I. W. and Rothwell, R. G. (2006) 'A geochemical application of the ITRAX scanner to a sediment core containing eastern Mediterranean sapropel units', Geological Society, London, Special Publications. Geological Society of London, 267(1), pp. 65–77. doi: 10.1144/GSL.SP.2006.267.01.05.

University, C. (no date) Stable Isotopes. Available at: http://www.columbia.edu/~vjd1/stable_isotopes.htm (Accessed: 4 June 2018).

Vorren, T. O. and Laberg, J. S. (1996) 'Late glacial air temperature, oceanographic and ice sheet interactions in the southern Barents Sea region'. Available at: http://sp.lyellcollection.org/content/specpubgsl/111/1/303.full.pdf (Accessed: 28 May 2018).

Vorren, T. O., Hald, M. and Lebesbye, E. (1988) 'Late Cenozoic environments in the Barents Sea', 3(5), pp. 601–612. Available at: https://agupubs.onlinelibrary.wiley.com/doi/pdf/10.1029/PA003i005p00601 (Accessed: 7 May 2018).

Walker, M. et al. (2009) 'Formal definition and dating of the GSSP (Global Stratotype Section and Point) for the base of the Holocene using the Greenland NGRIP ice core, and selected auxiliary records', Journal of Quaternary Science. Wiley-Blackwell, 24(1), pp. 3–17. doi: 10.1002/jqs.1227.

Weltje, G. J. and Tjallingii, R. (2008) 'Calibration of XRF core scanners for quantitative geochemical logging of sediment cores: Theory and application', Earth and Planetary Science Letters. Elsevier, 274(3–4), pp. 423–438. doi: 10.1016/J.EPSL.2008.07.054.

What Are 'Proxy' Data? | National Centers for Environmental Information (NCEI) formerly known as National Climatic Data Center (NCDC) (no date) National Centers for Environmental Information (NCEI) formerly known as National Climatic Data Center (NCDC). Available at: https://www.ncdc.noaa.gov/news/what-are-proxy-data (Accessed: 1 June 2018).

Winsborrow, M. C. M. et al. (2010) 'Deglaciation of a marine-based ice sheet: Late Weichselian palaeo-ice dynamics and retreat in the southern Barents Sea reconstructed from onshore and offshore glacial geomorphology', Quaternary Science Reviews. Pergamon, 29(3–4), pp. 424–442. doi: 10.1016/J.QUASCIREV.2009.10.001.

Wollenburg, J.E. and Mackensen, A., 1998. Living benthic foraminifers from the central Arctic Ocean: faunal composition, standing stock and diversity. Marine Micropaleontology, 34(3), pp.153-185.

Wollenburg, J. E., Knies, J. and Mackensen, A. (2004) 'High-resolution paleoproductivity fluctuations during the past 24 kyr as indicated by benthic foraminifera in the marginal Arctic Ocean', Palaeogeography, Palaeoclimatology, Palaeoecology, 204(3–4), pp. 209–238. doi: 10.1016/S0031-0182(03)00726-0.

Wollenburg, J. E., Kuhnt, W. and Mackensen, A. (2001) 'Changes in Arctic ocean paleoproductivity and hydrography during the last 145 kyr: The benthic foraminiferal record', Paleoceanography, 16(1), pp. 65–77. doi: 10.1029/1999PA000454.